Theses and Dissertations

8-2017

Intravenous Administration of Iron Oxide Nanoparticles in the Chicken Model

Huong Thi Ngoc Le
University of Arkansas, Fayetteville

Intravenous Administration of Iron Oxide Nanoparticles in the Chicken Model

A thesis submitted in partial fulfillment
of the requirements for the degree of
Master of Science in Cell and Molecular Biology

by

Huong Thi Ngoc Le
University of Science
Bachelor of Science in Biotechnology, 2011

August 2017
University of Arkansas

This thesis is approved for recommendation to the Graduate Council

_____
Gisela F. Erf, Ph.D.
Thesis Director

_____
Charles F. Rosenkrans Jr., Ph.D.
Committee Member

_____
Timothy J. Muldoon, Ph.D.
Committee Member

ABSTRACT

To be used in health care, the safety and effectiveness of nanoparticles needs to be tested in a living organism. The objective of this project was to develop the chicken as a convenient animal model to examine tissue targeting of intravenously (i.v.)-injected iron oxide (IO) nanoparticles. In Experiment 1, different doses of IO-COOH were i.v. injected into chickens; blood was collected at 0, 5, 15, 30, and 60 minutes post-injection; liver, spleen, lung, and kidney were collected after the last blood collection. For Experiment 2, IO-COOH and IO-PEG were i.v. injected into chickens; blood and the organs were collected at 0, 5, 15, 30, and 60 minutes post-injection. For both Experiments, IO concentration in blood was examined by iron test kit and fixed tissue sections were stained with H/E and Prussian blue stain. Portions of organs from Experiment 2 were frozen and used for preparation of homogenates and tissue-sections for immunohistochemical and/or iron-staining. For Experiment 3, the dermis of growing feathers (GF) was injected with mouse-IgG antigen (Ag); 6 hours later, IO-Ab (IO-COOH conjugated with chicken-antibody specific for mouse IgG), IO-COOH, or IO-PEG were i.v. injected into the chickens; one Ag-injected GF and one uninjected GF per chicken was collected at 0, 0.1, 0.5, 1, 2, 24, and 48 hours post-i.v.-injection; organs were collected at three and seven days post-i.v.-injection; and tissue sections of GFs and organs were stained with Prussian blue stain. Together, results of Experiment 1 and Experiment 2 revealed that IO-nanoparticles were taken up quickly by macrophages in liver and spleen, whereby IO-PEG was taken up at lower levels and slower pace by phagocytic cells when compared to IO-COOH. Experiment 3 was not successful in demonstrating delivery of intravenously injected IO nanoparticles to antigen-injected GFs. This may be due to the low dose of nanoparticles injected as well as the antigen-antibody system used. This is the first report describing organ-distribution and uptake of i.v. injected IO

nanoparticles in the chicken system, setting the stage for using the avian model to test *in vivo* targeting effectiveness of nanoparticles.

ACKNOWLEDGEMENT

I would like to express my special thanks of gratitude to my respected advisor Dr. Gisela F. Erf for all the things she has done for me. She gave me the opportunity to study in the U.S. and to do this wonderful project as well as guided me with all her enthusiasm.

I am grateful to Dr. Charles F. Rosenkrans, Jr., and Dr. Timothy J. Muldoon for being my committee members.

I wish to express my thanks to my lab-mates Hyeonmin Jang, Daniel Falcon, and Kallie A. Sullivan, who helped me during the time I conducted this project.

I would like to thank my very kind neighbors, aunt Kim and uncle Calvin, for helping us, and taking care of my daughter when I and my husband were busy with studying.

I take this opportunity to record sincere gratefulness to my parents, my mother-in-law, and my father-in-law for supporting and encouraging me to pursue my dream.

Specially, I would like to thank my husband Khue Nguyen who is always by my side to take care of me, support, and energize me, and thank my little daughter Maggie Nguyen who always brings happiness to our family so that I was in the best mood to study and completed this project.

TABLE OF CONTENTS

LIST OF ABBREVIATIONS

aka	as known as
d	Day
DAB	3 3'-Diaminobenzidine Tetrahydrochloride
FDA	Food and Drug Administration
GF	Growing Feather
h	Hour
H/E	Hematoxylin and Eosin stain
i.d.	Intradermal Injection
i.v.	Intravenous
IgG	Immunoglobulin G
IHC	Immunohistochemistry
IO	Iron Oxide
IO-COOH	Carboxylic Linked Iron Oxide
IO-PEG	Poly-ethylene-glycol Coated Iron Oxide
LBL	Light-brown Leghorn
MHC	Major Histocompatibility Complex
min	Minute
MPS	Mononuclear Phagocytic System
O.C.T	Optimal Cutting Temperature
OD	Optical Density
PBS	Phosphate Buffered Saline
SPION	Superparamagnetic Iron Oxide Nanoparticle

LIST OF FIGURES

LIST OF TABLES

<center>**LITERATURE REVIEW**</center>

1. Introduction

Nanoparticles have been extensively studied for various biomedical applications. One goal of nanotechnology is to use nanoparticles for delivery of drugs and toxins to target cells, such as tumor cells for example. Nanoparticles possess ability to carry antibodies, nucleotide probes, lectins, and other molecules, allowing specific interaction between probe carrying nanoparticles and target molecules. Numerous studies are carried out to develop nanoparticle targeting strategies, including modifications that hide the particle from the immune system, allow it to cross the endothelial cell blood barrier, keep it intact until it enters the target tissue, or cause it to undergo desired changes by the time it reaches the target tissue (Koo et al., 2011; Yang et al., 2008; Sajja et al., 2009).

To be used in health care, the safety and effectiveness of nanoparticles needs to be tested in a living organism. The skin and its living derivatives such as foot pad, ear lobes, toe web, wattle, and wing web have been used as valuable test-sites in both mammalian and avian species to examine tissue responses to a variety of materials injected into this complex tissue in living animals (Erf and Ramachandran, 2016). Even in human medicine, the skin is used to determine exposure or sensitization to antigen (e.g. tuberculin test, allergy test) (Crawford, 2017; Nickels et al., 2014). Intradermal injection of test-material generates a visible response that can be assessed based on the time course of the reaction and the presence of edema, induration, redness, and other visible or palpable characteristics (Chin et al., 2013). However, in animal testing information on cellular and molecular interactions that occur within a complex tissue is only available upon invasive biopsy or post-mortem sampling of the tissue, greatly reducing the

opportunity for monitoring events over time in the same individual (Falzarano et al., 2014; Bai et al., 2013; Ulbrich et al., 2011).

For the avian model, the growing feather has been identified as a convenient skin derivative for *in vivo* testing of test-materials. In chickens, the living portion of two- to three-week-old growing feathers is a column of pulp, which is approximately 8-10 mm in height with a 2-3 mm diameter. The pulp consists primarily of dermal tissue bordered by an epidermal layer. It contains the vascular supply of the growing feather and is an immunologically active site capable of recruitment of leukocytes and soluble factors from the circulation (Lucas and Stettenheim, 1972; Erf and Ramachandran, 2016). In addition, the growing feather can easily be removed by pulling it from its follicle, providing a tissue biopsy that is defined in size and structure without surgery. In recent years, Erf and colleagues (Erf and Ramachandran, 2016; Erf et al., 2017; Sullivan and Erf, 2017; US Patent 8,216,551, 2012) have established the growing feather as a suitable and defined dermal test-site providing insight into local immune system/tissue activities to test-material injected into the dermis of the pulp. Both injection and collection of growing feathers are considered minimally invasive procedures. Multiple growing feathers can be injected at one time in the same individual and then they can be collected at various time points post-injection for *ex vivo* analysis. Therefore, the chicken growing feathers are suitable for minimally invasive examination of biological activities of nanoparticles *in vivo*. It is likely that the feather injection method can also serve as a window into the effectiveness of nanoparticle targeting. If antigen placed into the feather pulp can attract immune components to enter the pulp tissue, it should also allow circulating nanoparticles coated with antigen-specific antibodies to come to the target site to interact with antigen.

The overall goal of this thesis research was to explore the suitability of the avian growing feather as a tissue test-site to monitor targeting of intravenously administered nanoparticles that are coated with antigen-specific antibody to the tissue-site where the antigen is located. In this model, the antibody-conjugated nanoparticle will be intravenously administered to the chicken and the antigen will be injected into the dermis of the chicken's growing feathers. The antigen-injected growing feathers will then periodically be sampled and examined for the presence of nanoparticles. The nanoparticle chosen for this project are iron oxide nanoparticles (10 nm), the target antibody is chicken IgG specific to mouse IgG, and the target antigen is mouse IgG. While immune activities in response to intradermal injection of growing feathers with of mouse IgG have previously been examined, intravenous injection of iron oxide nanoparticles in chickens has not. Therefore, a major part of this study is to examine the organ-distribution and circulatory half-life of intravenously injected iron-oxide nanoparticles in the chicken, before the targeting studies can be carried out.

2. Nanoparticle Delivery/Targeting

Nanoparticles can be described as nanometer size particles which are used as tiny probes to track the cellular machinery with minimally physical interference to cells (Taton, 2002). Nanoparticles can be conjugated with biological molecules which favor their interaction with cellular or molecular targets. A variety of biological molecules consisting of antibodies and biopolymers can be tagged on nanoparticles (Sinani et al., 2003). Nanoparticles demonstrate various structures such as sphere, rod, and platelet-like shape which can be used in biological systems for transportation of drug-conjugated nanoparticles to targets (Rodzinski et al., 2016).

Nanoparticles are used for a wide range of applications, especially for drug and gene delivery (Salata, 2004). For example, doxorubicin liposomes (aka Doxil) and 130 nm albumin-bound particle formulation of paclitaxel (aka Abraxane) are nanoparticles used as delivery systems for small-molecule drugs that are currently available in the pharmaceutical market (Mitragotri et al., 2014). Doxil is being used as medication for ovarian cancer and AIDS-related Kaposi's sarcoma (Barenholz, 2012). It was approved by the US Food and Drug Administration (FDA) in 1995 and became the first nano-drug to be sold in the USA and Europe. The Doxil nano-liposomes are comprised of hydrogenated soya phosphatidylcholine, cholesterol, and poly ethylene glycol (PEG)-modified phosphatidylethanolamine at 55:40:5 molar ratio (Abraham et al., 2005). This liposome design gives Doxil important advantages as a drug delivery system because the PEG-modified phosphatidylethanolamine increases the circulation time of Doxil and helps it escape the activity of the reticuloendothelial system. Additionally, an ammonium sulfate gradient was used as a driving force for the efficient and stable loading of doxorubicin into liposomes (Barenholz, 2012). Abraxane, a second-line treatment therapy for breast cancer patients (Von Hoff et al., 2013) is the combination of nano-scale albumin and paclitaxel molecules (130-nm particle formulation) (Miele et al., 2009). Paclitaxel is an extracted product from the bark of *Taxus brevifolia* which is commonly used as medication for breast, lung, and advanced ovarian cancers (Rowinsky and Donehower, 1995). Albumin possesses attractive characteristics for being a drug delivery vehicle including: (1) it is a natural carrier of endogenous hydrophobic molecules which can be used for reversible non-covalent loading and for the drug releasing process, and (2) albumin has been shown to bind to cell surface receptors (gp60, osteonectin), which facilitate the drug loading process to targets (Hawkins et al., 2008; Tiruppathi et al., 1997).

Recently, superparamagnetic iron oxide nanoparticles (SPIONs) have drawn attention for drug delivery applications. SPIONs are quickly engulfed by cells of mononuclear phagocytic system, especially macrophages in liver, spleen, lymph nodes and bone marrow (Clemente-Casares and Santamaria, 2014). SPIONs can be easily generated in various size ranges such as very small iron oxide nanoparticles (<10 nm in diameter), ultra-small iron oxide nanoparticles (<50 nm in diameter), and standard iron oxide nanoparticles (50–500 nm in diameter) (Clemente-Casares and Santamaria, 2014). In addition, due to possessing magnetic properties (Mahmoudi et al., 2011), SPIONs have been applied to deliver drugs to specific target sites *in vivo* with an external magnetic field for treating cancer and autoimmune diseases (Alexiou et al., 2000; Clemente-Casares and Santamaria, 2014). The delivery process of drugs using SPIONs is established by the cooperation of forces exerted by the blood flow rate and magnetic forces generated from an external magnetic field (Mahmoudi et al., 2011). Currently, the magnetic field gradient is produced by a strong permanent magnet, such as neodymium magnet – a rare earth magnet, positioned outside the body above the target site. Drug/SPION (biocompatible ferrofluid) complexes are then administrated into the body of patients via the circulatory system. The drug/SPION complexes are retained at the target site when the magnetic force is greater than the linear blood flow rates in arteries (10 cm s−1) or capillaries (0.05 cm s−1) (Pedro et al., 2003). When the drug/SPION complexes are settled down at the target site, drugs can be released by enzymatic activity and/or physiological variations (pH, temperature) and then may be engulfed by endothelial cells at target tissues (Alexiou et al., 2000).

Iron oxide nanoparticles have many characteristics that make them popular for use in the biomedical field, especially because they can easily be detected in cells and tissues, which is a very important characteristic for the first investigation into uses of the avian test-system for

5

nanomaterial research. The Prussian blue assay is a useful staining method commonly used in determining the presence of iron oxide nanoparticle in tissues (Attaluri et al., 2015; Fu et al., 2016; Jarockyte et al., 2016; Rodrigues et al., 2017; Ungureanu et al., 2015). Based on their ability to catalyze oxidation reactions, iron oxide nanoparticles can also be detected in tissues making use of their peroxidase mimicking activity in a variety of peroxidase based assay systems (Bhuyan et al., 2015; Chaudhari, 2012; Woo et al., 2013; Zhuang et al., 2012). Iron oxide nanoparticles are commercially available and have been used in a variety of toxicology and immunology studies. Iron oxide is also approved for use in humans by the Food and Drug Administration (FDA) and has been shown in *in vitro* and *in vivo* studies to have no apparent toxic effects and little bioactivity (Lu et al., 2010). Some reports suggested that by itself iron oxide nanoparticles appear to initiate pro-inflammatory macrophage activity and influence the activities of T cells (Lartigue et al., 2012; Shen et al., 2011). Others reported no bioactivities of iron oxide nanoparticles when used to label *in vitro* activated dendritic cells in an effort to monitor their activities *in vivo* (Tavaré et al., 2011). However, with the proper modifications, such as addition of polymeric structures and linking of antigen, antigen conjugated iron oxide nanoparticles can modulate innate immune activity and the development of adaptive immunity specific to antigens conjugated to their surface (Pusic et al., 2013). Moreover, iron oxide nanoparticles can be modified to gain stealth properties (hide from immune system components), prolonging their circulatory half-life, influencing their distribution, and allowing for passive and targeted delivery of iron oxide nanoparticles to inflamed tissues and specific targets (Mahdavi et al., 2013; Mahmoudi et al., 2011; Muthiah et al., 2013; Sun et al., 2010; Strehl et al., 2016; Yuan et al., 2012).

Poly-ethylene-glycol (PEG) coating of iron oxide nanoparticle is one of the common modifications of iron nanoparticles due to its biocompatibility, reducing their capture by the body's immune system components. According to Yu and colleagues, PEG coated iron oxide nanoparticles are less engulfed by porcine aortic endothelial cells in 3D cell culture when compared with dextran coated iron oxide nanoparticles, increasing the chances of delivery of iron oxide nanoparticles via the blood stream to the target sites (Yu et al., 2012). Similarly, in another *in vitro* study, murine macrophages (RAW 264.7 cell line) took up three times more dextran coated iron oxide nanoparticles than PEG coated iron oxide nanoparticles (Chen et al., 2010). In addition, iron oxide nanoparticles are the potential candidates for drug delivery application because they can be modified to provide reactive sites suitable for further binding of drugs and biological ligands. For example, iron oxide nanoparticles could be linked to reactive carboxylic acid group which can be conjugated to protein, peptide and other amine containing molecules, allowing for specific interaction between the probe carrying nanoparticles and the target molecules (Pusic et al., 2013).

In a report by Zhuang and colleagues (Zhuang et al., 2012), the bio-distribution and organ clearance of iron oxide magnetic nanoparticles in mice model were quantitatively analyzed in order to understand the *in vivo* behavior of the nanoparticles. For this study, a histochemical method for identifying intravenously administered iron oxide nanoparticles in organs was developed based on the peroxidase mimicking activity of the nanoparticles enabling them to oxidize peroxidase substrates such as 3 3'-diaminobenzidine tetrahydrochloride (DAB) to form a brown colored precipitate at the site of the nanoparticle presence. Prussian blue assay also was carried out in this study to identify the presence of the iron oxide nanoparticles in the organs including liver, spleen, lung, kidney, lymph node, and thymus. The results showed that the

nanoparticle peroxidase staining was more sensitive than the Prussian blue staining. Based on images of Prussian blue and Hematoxylin- and Eosin-(H/E) stained adjacent tissue sections, the authors concluded that the nanoparticles were taken up by types of macrophages in liver, alveolar macrophages in lung, and macrophage in the perifollicular areas in spleen (Zhuang et al., 2012). The study would have been more significant if more direct proof were provided (i.e. dual iron oxide- and immuno-staining) regarding the cell-types that have taken up the iron oxide nanoparticles.

Rodrigues and his colleagues, in their articles, examined the number of macrophages in mouse liver and spleen engulfing intravenously injected iron oxide nanoparticles and reported that their number increased linearly depending on iron oxide dose. Iron oxide was deposited in all zones of the liver and in the marginal zone of the spleen, clarifying that liver and spleen were involved in the clearance pathways of iron oxide nanoparticles from the blood. In addition, the highest dose (50 mg/kg) of iron oxide was cytotoxic, but no significant effect was determined for the lower doses (8 mg/kg and 20 mg/kg) (Rodrigues et al., 2017).

3. Chicken Growing Feather

In birds, the growing/regenerating feather constitutes another living part of the integument. In chickens, the ensheathed living portion of a growing feather is approximately 8-10 mm in height with a 2-3 mm diameter. The living tissue of growing feathers is the pulp, which consists mainly of an inner dermis, which arose from the dermal papilla and consists of loose and pliable mesenchymal reticulum (Lucas and Stettenheim, 1972). The dermis is bordered by an epidermal layer, which arose from the epidermal collar of the follicle, and envelopes the column of dermis. The epidermis is modified at the base (3 mm of newest growth) into the

keratinocyte- and melanocyte-containing barb ridge. An outer connective tissue sheath surrounds the column of pulp and the first few millimeters of newly formed barbs. The feather pulp contains the vascular supply of the growing feather including a central axial artery and an extensive network of smaller arterioles, capillaries, small sinuses, venules and veins, as well as, lymphatic capillaries and vessels. The vascular system is well able to adjust the pressure and volume of blood flow at various levels. Additionally, the feather pulp dermis is an immunologically active site capable of recruitment of leukocytes from the circulation and has a sparse mononuclear cell presence similar to that observed in the dermis of the skin (Abdul-Careem et al., 2008; Erf et al., 1995). Growing feathers can be easily removed from the skin because unlike mature feathers they are not firmly anchored in the skin, and collection of samples is considered minimally invasive, similar to sampling the peripheral blood. Moreover, using regenerating growing feathers of the same age for injection, the amount of tissue obtained is uniform over the time-course of a study for all treatments (Erf and Ramachandran, 2016).

The growing feather has been developed as a skin test tissue to monitor and assess cellular/tissue responses to various test-materials including polypeptides, polynucleotides, carbohydrates, microbes, chemicals and other agents, especially nanoparticles (US patent 8,216,551, 2012). The comparison of the leukocyte profiles in growing feathers, wattles, and wing web following intradermal injection of *Mycobacterium butyricum* showed clear similarities in the time-course, quantity, and type of leukocytes (T helper cells, cytotoxic lymphocytes, B cells, and MHC class-II positive cells) recruited from the blood to the site of *M. butyricum* injection for all three dermal test-sites. Moreover, the manipulating steps after collection of injected tissues, including cutting, staining, and examination of frozen tissue sections, were much less difficult for growing feathers than for the other tissues (Erf and Ramachandran, 2016).

In addition to the unique features of the growing feather dermal test-site, the chicken model has other characteristics that make it an important animal model for biomedical research. The ability to concurrently conduct repeated sampling of blood and injected growing feathers using minimally invasive procedure provides a powerful and unique model system for *in vivo* study of nanoparticles bioactivity. While some aspects of the immune system differ from those of the mammalian immune system, the soluble and cellular components of the innate and adaptive immune systems, as well as, their functional activities are highly similar between chickens and humans (including, leukocytes and soluble factors of innate immunity, antigen presentation, T and B lymphocyte subpopulations, effector and memory responses, hypersensitivities, etc.) (Davison et al., 2008; Wick et al., 2010). The chicken genome was the first genome of a food animal to be sequenced, providing research tools and opportunities in line with biomedical research; additionally, antibodies and other reagents for immunological research in the avian system are readily available and continue to be developed at a rapid pace. A variety of human diseases including spontaneous autoimmune diseases (e.g. vitiligo, Hashimoto's thyroiditis, and scleroderma), cancer (e.g. ovarian, lymphoma, Rous sarcoma) and infectious diseases are being investigated using the chicken as the animal model (Wick et al., 2006).

Based on the above described properties of the growing feather, preliminary results from growing feather injections of test-materials, and the valuable characteristics of the chicken model, we can expect that the growing feather constitutes a complex integumental tissue suitable for *in vivo* assessment and minimally invasive monitoring of toxicity and bioactivities of nanoparticle *in vivo*, including monitoring the deliver/targeting of nanoparticles administered intravenously.

4. Objectives

The overall objective of this study was to develop the chicken as a convenient animal model to examine tissue targeting of intravenously injected nanoparticles. Specifically, it was hypothesized that using antigen-injected growing feathers as the target tissue, arrival and bioactivities of antigen-specific nanoparticles injected into the blood circulation could be monitored by *ex vivo* analyses of antigen-containing growing feathers collected at various times after the intravenous administration antigen-specific nanoparticles.

The proposed nanoparticle used for this project was iron oxide (10 nm), the target antigen was mouse IgG, and the antigen-specificity of the iron oxide nanoparticles was achieved by conjugating them with mouse IgG-specific chicken antibody. This nanoparticle, antigen, and antibody system was chosen based on ongoing studies in our laboratory. While local pro-inflammatory activities (including vascular changes favoring recruitment of soluble factors and cells from blood into the tissue) of mouse IgG injected into the dermis of growing feathers was previously shown (Erf, personal communication; Erf et al., 2017), in vivo activities of intravenously injected nanoparticles have not been examined in chickens. Therefore, a major part of this study was first to examine the organ-distribution and circulatory half-life of intravenously injected iron oxide nanoparticles in the chicken, before the targeting studies could be carried out.

In Experiment 1, the dosage, time-course of detection in the peripheral blood circulation and uptake from the blood into organs of intravenously injected iron oxide nanoparticles were examined. Different doses of iron oxide nanoparticles were intravenously injected into the wing veins of chickens. Blood was collected before (0), and at 5, 15, 30 and 60 min post injection. After the last blood collection, the chickens were euthanized for organ (spleen, liver, kidney and lung) collection. Iron oxide concentration in blood was then examined by commercial iron test

kit. Collected organs were processed and tissue sections stained with H/E stain and Prussian blue iron stain for histological analysis.

For Experiment 2, one dosage of two different iron oxide nanoparticles was intravenously injected into the wing veins of chickens. Blood and organs were collected before (0), and at 5, 15, 30 and 60 min post injection. Iron oxide concentration in blood was then examined by commercial iron test kit. Processed tissues were sectioned and stained with H/E and Prussian blue iron stain. Frozen organs were used for preparation of homogenates, immunohistochemical staining, and iron staining in an effort to determine organ and cellular distribution of nanoparticles, as well as the type of cell involved in IO nanoparticle uptake.

For Experiments 3, antigen (mouse IgG) was intradermally injected into the pulp of several growing feathers of chickens. Six hours later, iron oxide nanoparticles conjugated with chicken antibody specific for mouse IgG were intravenously injected into the wing veins of chickens. The antigen-injected growing feathers were collected before (0), and at 0.1, 0.5, 1, 2, 24, and 48 h post-intravenous injection of nanoparticles. Birds were euthanized at 3 d and 7 d post intravenously injection for organ collection. Tissue sections of the collected growing feathers and organs were prepared and stained with Prussian blue stain for histological analysis.

MATERIALS AND METHODS

1. Experimental Animals

Chickens used in this experiment were 8- or 9-week-old females from the Light Brown Leghorn (LBL) line of chickens maintained by G. F. Erf at the University of Arkansas Poultry Farm, Division of Agriculture. On the day of hatch, each bird was tagged using numbered labels. Chicks were not vaccinated, and moved to a HEPA-filtered room in the Arkansas Experiment Station Poultry Health Laboratory in Fayetteville, Arkansas. The chicks were placed in floor pens on wood shavings litter, 10-12 chicks per pen, with food and water available *ad libitum* (Shi et al., 2012). The chicks were then shown the location of food and how to drink water from the water nipples. Food, water, and the wellbeing of the chicks were checked every day. The pens as well as the animal room were dusted daily and the floor of the room washed to maintain a clean environment for chicks to grow. The temperature settings in the room were 36.1 $^{\circ}$C from day 1-7, 30 $^{\circ}$C from day 8-14, 26 $^{\circ}$C from day 15-21, and 23 $^{\circ}$C from day 21 until the end of the experiment. Additionally, each pen was equipped with one infrared heat lamp for the first week. The light-dark schedule was 24 h light from day 1-5 and then 15 h of light with 9 h of dark until day 42, and 10 h light to 14 h of dark thereafter. All protocols involving animals were approved by the University of Arkansas Institutional Animal Care and Use Committee (IACUC Protocol #15022).

2. Iron Oxide Nanoparticles used in this Study

There were three kinds of iron oxide nanoparticles used in this project, including 10 nm Fe_2O_3 with carboxylic acid groups (IO-COOH, 5 mg/mL, Ocean NanoTech, LLC, Springdale, Arkansas), polyethylene glycol-coated iron oxide nanoparticles (IO-PEG, 1 mg/mL, Ocean

NanoTech), and chicken-anti-mouse IgG antibody-coated iron oxide nanoparticles (IO-Ab, 5 mg/mL). The conjugation of chicken-anti-mouse IgG antibodies (Rockland) to IO-COOH was carried out by Zystein LLC, Fayetteville, Arkansas at a ratio of 1:2.5.

IO-COOH is a group of water soluble iron oxide nanoparticles with amphiphilic polymer coating. Their reactive group is carboxylic acid and their zeta potential is from -35 mV to -15 mV. Their organic layers consist of a monolayer of oleic acid and a monolayer of amphiphilic polymer. The overall thickness of the organic layers is about 4 nm. The hydrodynamic size of the nanoparticles is about 8-10 nm larger than their inorganic core size measured by TEM. IO-COOH is very stable in most buffer solutions in the pH range of 4-10. It can be conjugated to protein, peptide and other amine containing molecules (Ocean NanoTech, Specification Sheet).

IO-PEG is a group of water soluble iron oxide nanoparticles with amphiphilic polymer and PEG coating. There is no linkable reactive group on the surface of nanoparticles. The zeta potential of IO-PEG is from -10mV to 0. The thickness of the total organic layers is about 6 nm. The hydrodynamic size of the nanoparticles is about 12-14 nm larger than their inorganic core size measured by TEM. The colloidal stability of IO-PEG is exceptionally high. It is stable in most buffer solutions in the pH range of 4-10 and can survive autoclaving process (121 ºC for 30 min) (Ocean NanoTech, Specification Sheet).

3. Experiment 1: Intravenous Injection of Different Doses of IO-COOH

For intravenous injection, the stock of IO-COOH nanoparticles was diluted to 4.5 mg/mL using endotoxin-free Dulbecco's Phosphate-buffered Saline (PBS, Sigma, Chemical Company,

St. Louis, MO). Different dosages of IO-COOH were intravenously injected into the left wing vein of 9-week-old female LBL chickens. Dosages ranged from 2.4-2.8 mg/kg (low dose; n = 3 chickens) to 5.4-5.7 mg/kg (high dose; n = 2). Additionally, 3 chickens were injected with 0.5 mL of PBS to serve as the vehicle injection control.

Before injection, the chickens were weighed and the right wing vein rinsed with 70 % alcohol. The right wing vein was then injected with the IO-COOH nanoparticles or vehicle using 1 mL syringes with 0.1 mL gradation and 25 gauge x 1 inch needles (BD; Becton, Dickinson, and Company, Franklin Lakes, NJ), respectively. For blood collection, 0.5 mL of blood was collected from the wing veins into heparinized 1 mL syringes with 25 x 1 needles (BD) before (0), and at 5, 15, 30, and 60 min post-intravenous IO-COOH injection. To avoid hematoma, pressure was placed on the vein after withdrawal of the needle until bleeding stopped and use of the left- and right-wing veins were alternated between blood samplings. The blood was then used for preparation of plasma.

To examine organ distribution of i.v. injected IO-COOH, the organs including spleens, livers, kidneys, and lungs were collected after the last blood collection (60 min time-point). For organ collection, chickens were euthanized by i.v. injection of pentobarbital (Sigma Aldrich) solution (1 mL of 65 mg/mL) and the organs were removed. Half of each organ was put into a 100 mL plastic specimen cup containing 40 mL of 10% formalin solution, the other half was wrapped in labeled aluminum foil, snap frozen in liquid nitrogen, and stored at – 80°C.

4. Experiment 2: Intravenous Injection of IO-COOH and IO-PEG at the Same Dose

The dose of IO-COOH and IO-PEG injected in this experiment was 1.5 mg/chicken (approximately 3.3 mg/kg, n = 3 chickens). Because the stock of IO-PEG was only 1 mg/mL, 3 mL syringes with 25 x 1 needles were used to inject the 1.5 mg in a 1.5 mL volume. Four chickens were injected with 1.5 mL of PBS (vehicle control). All other aspects regarding injection procedure were as described for Experiment 1. For Experiment 2, blood was collected as in Experiment 1, although no anti-coagulant was used in Experiment 2. The blood was allowed to coagulate for preparation of serum. Additionally, for Experiment 2, organs were collected and processed as described in Experiment 1, except chickens were euthanized for organ collection before (0) and at different times post-injection [0 (n=2), 5 (n=3), 15 (n=3), 30 (n=3), and 60 min (n=3)].

5. Experiment 3: Delivery/Targeting of IO-Ab (IO Coated with Chicken-anti-mouse IgG Antibody)

5.1. Preparation of growing feathers for injection

In this experiment, the target antigen, mouse IgG, was injected into the dermis of growing feathers of 8-week-old LBL female chickens 6 h before intravenous injections of iron oxide nanoparticles. Growing feathers were prepared for mouse IgG/PBS injection by cutting off the barbs that were emerging from the sheath, leaving about 2-3 mm of sheath above the epidermis of the pulp column. This approach helped with the injection procedure by ensuring that the fully inserted needle (8 mm), and therefore the injected solution, was about half way into the column of the GF dermis, and the injected GFs with cut barbs were easy to identify at the time of collection.

16

5.2. Preparation of syringes for intradermal injection of mouse IgG into growing feathers

On the day of injection, mouse IgG was diluted with PBS (Sigma, Chemical Company) to yield a concentration of 1 mg/mL. The mouse IgG solution or PBS was then aseptically added to 0.3 mL syringes with 0.01 mL gradation and 31 gauge x 8 mm needles (BD; Becton, Dickinson, and Company, Franklin Lakes, NJ) in a NuAir Biological Safety Cabinet (NuAir, Plymouth, MN). To load the syringes, which had non-detachable needles, the plunger was removed. Holding the syringe vertically, 220 µL of mouse IgG/PBS was added with a micropipettor to the back opening of the syringe. The solution was allowed to enter the syringe column until a 5 mm space was cleared below the top opening. The syringe was then quickly rotated 180^0 to let the mouse IgG/PBS solutions flow in the opposite direction, towards the syringe's back opening. Before the mouse IgG/PBS solution was flowing out of the syringe, it was stopped by contact with the head of the syringe plunger, and the plunger was reinserted into the syringe. The mouse IgG/PBS was then pushed towards the syringe needle until a tiny bubble of liquid formed at the needle opening. This loading technique was very successful in avoiding air bubbles in the syringe. The syringes were kept at room temperature and used within 2 h of preparation (Erf et al., 2017).

5.3. Injection of growing feathers with target antigen (mouse IgG) and intravenous injection of IO-nanoparticles

The basic protocol for this experiment is outlined in the diagram shown in Figure 1. For each chicken, 14 GFs were injected with 10 µL of mouse IgG (1 mg/mL) target antigen, 7 GFs on each the left and right breast tract. [Based on preliminary studies, intradermal injection of mouse IgG at this concentration and volume into the dermis of GFs results in vascular changes

that allow for significant recruitment of leukocyte and soluble factors from the blood to the site of mouse IgG injection (GF dermis) within 6 hours (Erf personal communication)]. Six hours after injection of the antigen into GFs, the iron oxide nanoparticles including IO-Ab (2.5 mg/bird, n = 5), IO-COOH (2.5 mg/bird, n = 3), and IO-PEG (1.5 mg/bird, n = 2) were intravenously injected in a 1.5 mL volume into the left wing vein of the chickens using 3 mL syringes with 0.1 mL gradation and 25 x 1 needles (BD). Injected GFs and uninjected GFs were collected before (0 h) and at 0.1, 0.5, 1, 2, 24, 48 h post intravenous injection. Two growing feathers per bird were collected at each time point. One of the two GFs was cut just below the epidermal cap and put into a 15 mL micro-centrifuge tube containing 1 mL of 10 % buffered formalin solution, the other one was placed into a labeled aluminum cup, covered with Tissue Tek$^{®}$ O.C.T. compound (Sakura Fine Tek USA, Inc, Torrance, CA, USA; VWR catalogue number 25608-930), snap frozen in liquid nitrogen, and stored at -80°C. Three days and 7 days post intravenous injection, half of the birds from each treatment were euthanized by i.v. injection of pentobarbital (Sigma Aldrich) solution (1 mL of 65 mg/mL), and the organs including spleen, liver, kidneys, and lungs were removed. The organs were cut into 2 portions, one portion was put into a 100 mL plastic lidded cup containing 40 mL of 10% formalin solution, the other portion of all tissues was wrapped in labeled aluminum foils, snap frozen in liquid nitrogen, and stored at -80°C (Figure 1).

6. Preparation of Plasma from the Heparinized Blood Samples

The heparinized blood samples collected for Experiment 1 were placed into 1.5 mL tubes and centrifuged at 7000 x g for 3 min using a microcentrifuge. After centrifugation, the supernatant plasma was collected and placed into 0.6 mL labeled tubes using a 20-200 µL

micropipettor with yellow tips. The cell pellets also were keep for future research. All of the samples were stored at -20°C.

7. Preparation of Serum from Blood Samples

The blood samples contained in 1.5 mL tubes from Experiment 2 were allowed to coagulate for 1 h at room temperature. The coagulated blood samples were then centrifuged at 4000 x g for 10 min using a swing bucket centrifuge. After centrifugation, the supernatant fluid (serum) was collected and transferred into new 1.5 mL labeled tubes using a micropipette with yellow tips. The pellets also were keep for future research. All of the samples were stored at -20°C.

8. Homogenization of Frozen Tissues

The 150 mg pieces of frozen livers from Experiment 2 were cut into small pieces and placed into 5 mL Falcon tubes (BD) containing 1500 μL assay buffer (Iron assay kit, Sigma Aldrich). The liver pieces were homogenized using a hand homogenizer for 5 min until there were no small pieces in the buffer. The homogenized solution then was transferred into 1.5 mL tube to be centrifuged at 13000 x g, at 4°C for 10 min. The pellet was discarded, the supernatant was obtained and used for iron assay.

9. Determination of Iron Concentration using Iron Assay Kits

Two commercial iron assay kits (Sigma Aldrich kit and BioChain kit) were used to identify concentration of iron in plasma, serum, and homogenized frozen tissues collected from

Experiment 1 and Experiment 2. In order to determine the IO concentration in these samples, experimental procedures described in Table 1 were carried out.

9.1. Sigma Aldrich iron assay kit

This is a quantitative colorimetric iron determination. Total iron including ferrous iron Fe^{2+} and ferric iron Fe^{3+} were measured at 593 nm. The linear iron detection range is 8-400 µM (0.45-22.34 µg/mL). The samples (plasma, serum, and homogenized tissue), iron assay buffer, iron probe, iron reducer, and iron standard were equilibrated to room temperature before use. A 1 mM standard solution was generated by diluting 10 µL of the 100 mM iron standard with 990 µL of distilled water. 0, 2, 4, 6, 8, and 10 µL of the 1 mM standard solution were added into wells of a 96 well plate to generate 0, 2, 4, 6, 8, and 10 nmole/well iron standards (1 mM = 1 mmole/L or 1 nmole/µL). The iron assay buffer was then added to these wells to bring the volume to 100 µL. The final concentrations of standards were 0, 0.02, 0.04, 0.06, 0.08, and 0.1 nmole/µL, respectively. Converted into ng/µL (or µg/mL), the concentration of standards were 0, 1.117, 2.234, 3.351, 4.468, and 5.585 ng/µL (or µg/mL), respectively. (iron atomic mass is 55.85 ng/nmole).

The plasma or serum samples were added to other wells of the same 96 well plate in triplicate, 100 µL of plasma or serum per well. 5 µL of iron reducer were then respectively added to the standard wells and sample wells. The solutions were mixed for 30 s using a shaker. The 96 well plate was then covered with aluminum foil to protect the standards and samples from light. All samples were incubated for 30 min at room temperature. After incubation, 100 µL of the iron probe was added to standard wells and sample wells. The wells were mixed for 30 s using the shaker. The plate was incubated for 60 min at room temperature, and then was measured at 593

nm wave length using a 96-well optical density (OD) plate reader. The OD values were recorded for analysis.

9.2. BioChain iron assay kit

This is a quantitative colorimetric iron determination. Total iron was measured at 590 nm. The linear iron detection range was 27-1000 μg/dL (0.27-10 μg/mL) iron. The concentration of iron oxide in serum, homogenized tissue samples were determined using iron assay kit (BioChain). The 400 μL of 1000 μg/dL Premix was prepared by mixing 40 μL of 10 mg/dL standard and 360 μL distilled water. The standards were generated by diluting 0, 10, 20, 30, 40, 60, 80, 100 μL of Premix with 100, 90, 80, 70, 60, 40, 20, 0 μL of distilled water, respectively. The final concentrations of standards were 0, 100, 200, 300, 400, 500, 600, 800, 1000 μg/dL, respectively (or 0, 1, 2, 3, 4, 5, 6, 8, 10 μg/mL, respectively).

Fifty μL of diluted standards and samples were added to a 96-well plate in triplicate. The Working Reagent was equilibrated to room temperature before use in the assay, and prepared by mixing 20 volumes of Reagent A, 1 volume of Reagent B and 1 volume of Reagent C. Once prepared, 200 μL of Working Reagent was added to well containing 50 μL of standards or samples, and 200 μL of Reagent A was added to the Sample Blank wells. The plate was tapped to mix the solutions. The 96-well plate was then covered with aluminum foil. All samples were incubated for 40 min at room temperature, and color development measured at 590 nm wave length using the OD plate reader. The OD values were recorded for analysis.

10. Preparation and Staining of Tissue Samples with Prussian Blue or Hematoxylin/Eosin Stain

The formalin-fixed organ samples from Experiment 1 and 2, and the formalin-fixed growing feather samples from Experiment 3 were processed, paraffin embedded, sectioned (5 µm) and stained with Prussian blue iron stain and violet red nuclear counterstain or Hematoxylin/Eosin (H/E) stain by David Cross at the University of Arkansas, Division of Agriculture Histology Service Laboratory housed in the Center of Excellence for Poultry Science, Fayetteville, AR.

11. Examination of Prussian Blue (Iron Stain) Stained Tissue Sections of Organs Collected from Chickens after intravenous Injection of Iron Oxide Nanoparticles

Two methods were used to quantify the iron staining:

11.1. Quantification of blue staining using image analysis

Twenty microscope fields per tissue section were examined at 400 x magnification using an Olympus BX50 light microscope (Olympus, Center Valley, PA) equipped with a CoolSNAP Pro digital camera (Media Cybernetics, Silver Springs, MD) and computer connection (Meyer Instruments, Houston, TX, USA). The blue color staining reflecting Prussian blue staining within each image (1 image per microscope field) was identified and quantified by image analysis using Image Pro Software. The data were expressed as % Area (blue area/image). Pictures of blue cell areas at 100 x and 400 x magnification were also taken using the system.

11.2. Quantification of blue stained cells using a bright-field microscope with an ocular 10 mm x 10 mm grid insert (manual counting method)

Using a bright field microscope (Olympus, Center Valley, PA), 20 randomly selected microscope fields per tissue section were examined and at 400 x magnification. Blue cells were counted with the aid of a 10 mm x 10 mm ocular grid insert with 100 subdivisions. The data were expressed as iron$^+$ cell per 62500 μm^2. Pictures of iron$^+$ blue cells at 100 x and 400 x magnification were taken using an Olympus BX50 light microscope (Olympus, Center Valley, PA) equipped with a CoolSNAP Pro digital camera (Media Cybernetics, Silver Springs, MD) and computer connection (Meyer Instruments, Houston, TX, USA).

12. Iron Staining of Frozen Tissues using the Peroxidase Mimicking Activity of Iron Oxide Nanoparticles

The frozen tissues (spleen, liver, kidney, lungs) were placed in O. C. T compound (Sakura Fine Tek USA and O.C.T. allowed to freeze at -23°C in a cryostat. Frozen tissue sections were then cut for histochemical staining using the cryostat. Identification of IO nanoparticles in frozen tissues making use of their peroxidase mimicking activity was reported in one publication by Zhuang et al. (2012). However, a detailed description of methods was not included in the publication and attempts to correspond with the author were not successful. Hence, many variations of the key steps in the procedure were carried out to optimize the staining method. The successful staining procedure was as follows: Seven-μm thick frozen sections were prepared using the cryostat and placed on microscope slides. The sections were incubated in 10% H_2O_2 (in 100% methanol) for 20 min, and then washed 3 times with 0.01 M PBS. The sections then were incubated in freshly prepared 3 3'-diaminobenzidine tetrahydrochloride (DAB) substrate solution

23

in the presence of 0.3% H_2O_2 overnight. The slides were washed with PBS 3 times and allowed to dry. The tissue sections on the slides were covered with 1 drop of Aqua-Mount mounting medium and covered with a glass coverslip.

13. Iron Staining for Frozen Tissues using HT20 Stain Kit (Sigma-Aldrich)

For iron staining using an iron staining kit, frozen 7 μm tissue sections of spleen and liver tissues were prepared as described above (12.). To optimize the iron staining procedure for frozen tissue sections, many combinations of key steps were tested. After optimization of the staining procedure for frozen tissue sections, the following procedure was used: The sections were incubated in a 10% H_2O_2 methanol bath for 20 min, and then washed 3 times with PBS. The working solution was prepared by mixing 20 mL of Potassium Ferrocyanide Solution (HT20 stain kit, Sigma-Aldrich) and 20 mL of Hydrochloric Acid Solution (HT20 stain kit, Sigma-Aldrich). The sections were incubated in the working solution for 10 min, and then were rinsed with deionized water. The sections were then counterstained with Pararosaniline (HT20 staining kit, Sigma-Aldrich) for 5 min, rinsed with deionized water and rapidly dehydrated through a series of alcohol and clearing (Clearing Agent; Electron Microscopy Sciences, Hatfield, PA) solutions. The tissue sections on the microscope slides were covered with a drop of Aqua-Mount mounting medium and covered with a glass coverslip.

14. Immunohistochemistry

To identify the leukocytes in the frozen tissue section that may have taken up IO nanoparticles, frozen tissues of spleen and liver were prepared as described above. Sections were fixed in acetone for 6 min, then incubated in 10% horse serum in PBS for 60 min. The sections

24

then were washed with PBS 3 times and incubated in 100 μL of separate primary mouse-monoclonal antibodies (all IgG1 isotype) specific to chicken macrophages (KUL-01), B cells (Bu-1), or MHC class-II. An isotype-staining control (mouse IgG1 with irrelevant specificity was also included. All primary antibodies, including the isotype control were prepared as 1 μL in 100 μL of horse serum) for 30 min. Then, the sections were washed 3 times with PBS, and quenched in a 10% H_2O_2 methanol bath for 20 min. After that, the sections were washed with PBS and incubated in 100 μL of secondary antibody which is biotinylated anti-mouse IgG (1 μL of secondary antibody in 100 μL of horse serum) for 30 min. The sections then were washed with PBS 3 times, and incubated in 100 μL of ABC reagent (1A : 1B : 100 PBS; Vekta) for 30 min. Freshly prepared DAB in the presence of 0.3% hydrogen peroxide was added to the slides, and sections incubated for 7 min. The slides then were washed 5 times with PBS, counterstained with Methyl green nuclear stain.

15. Variations of Immunohistochemistry and Prussian Blue Staining (HT20 kit) Double Staining Procedures for Frozen Tissue Sections

To determine what type of cells engulfed iron oxide nanoparticles, a staining procedure was developed combining the immunohistochemical and Prussian blue staining methods, whereby candidate cells including macrophages, B cells, and MHC class-II expressing cells were identified based on the brown color of the immunohistochemical staining and uptake of IO nanoparticles was determined by the blue color staining. To work out this double staining procedure modification of the individual staining procedures were required. In detail, the frozen sections were prepared and all the steps of immmunohistochemical staining were carried out as described above until the the DAB incubation step. Then, the sections were fixed in buffered

formalin solution for different lengths of time (0 min - no formalin fixation, 20 min, and overnight). After that, the sections were incubated in HT20 working solution (mixing of Potassium Ferrocyanide Solution and Hydrochloric Acid Solution) for 2 different time-points (10 min and overnight), and were then counterstained with Pararosaniline, washed with PBS, dehydrated and preserved by 1 drop of Aqua-Mount oil and covered with a glass coverslip.

16. Statistical Analyses

The experimental unit was the individual chicken. All statistical analyses were carried out using Sigma Plot 13 Statistical Software (Systat Software, Inc., San Jose, CA 95110). For Experiments 1, Pearson Correlation Analysis was conducted to determine the relationship between dosage of IO-COOH injected i.v. and amount (% Area) of iron staining in spleen and livers collected 60 min post IO-COOH injection. Similarly, for Experiment 2, Pearson Correlation analysis was used to compare the iron staining data obtained by image analysis (%Area) and manual counting of iron stained cells (# blue cells/62500 μm^2) in liver and spleen sections. One-way ANOVA followed by Fisher's LSD multiple mean comparisons was used to determine the effect of time post i.v. injection of IO nanoparticles on IO-nanoparticle uptake by liver and spleen. For all analyses, correlations and differences with P-values ≤ 0.05 were considered significant.
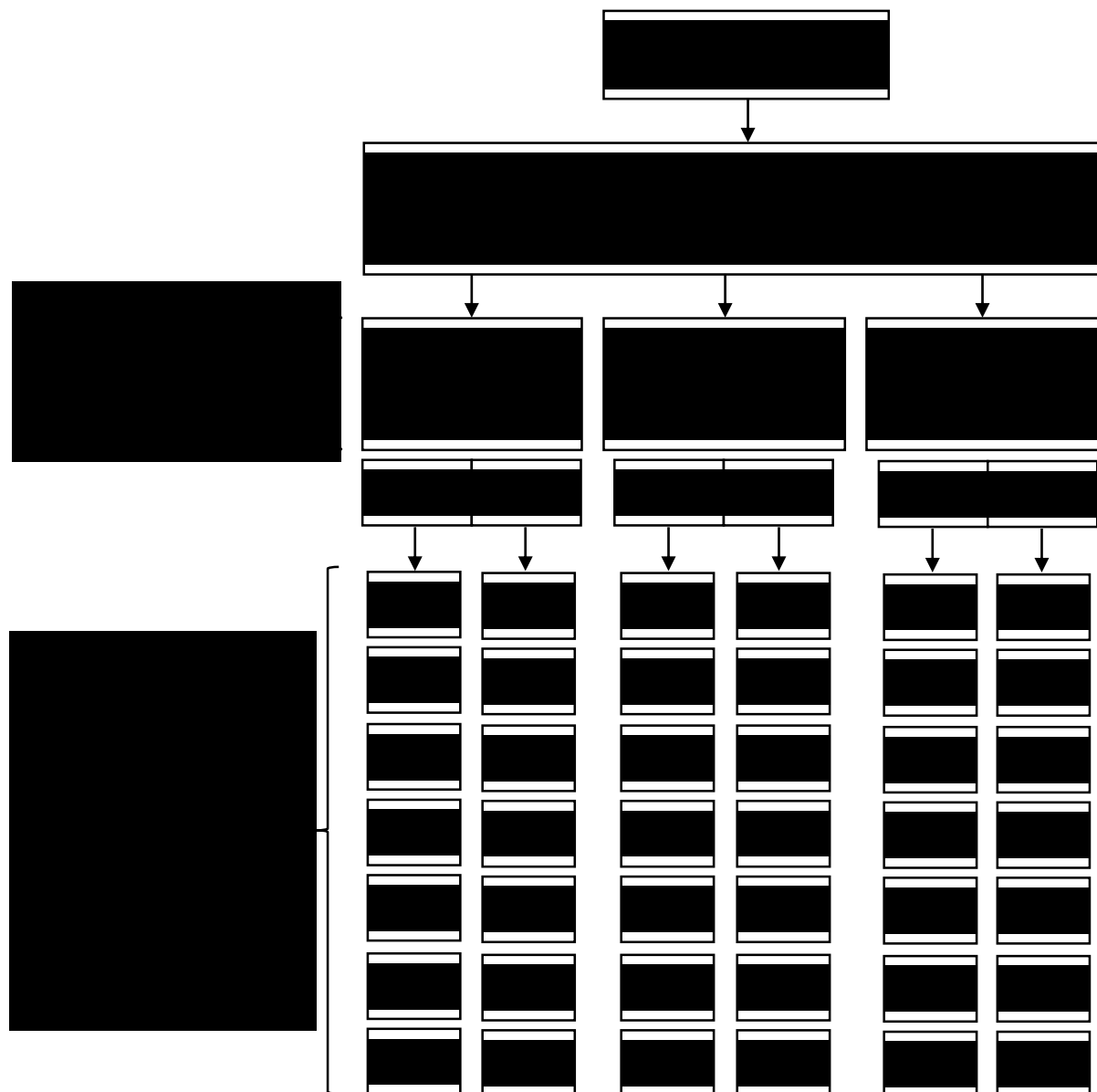
Figure 1. Summary of the protocol to study delivery/targeting of intravenously injected iron oxide (IO)-nanoparticles (NP) to the dermis of growing feathers (GF) injected with the target antigen (Ag; mouse IgG) in 8-week-old female Light-brown Leghorn (LBL) chickens. The dermis of 14 growing feather (GF) was injected with 10 μL of mouse IgG (1 mg/mL) target antigen. Six hours later, IO-Ab (IO conjugated with chicken antibody specific for mouse IgG, 2.5 mg /bird), IO-COOH (2.5 mg /bird), or IO-PEG (1.5 mg/bird) were intravenously injected into the wing veins of chickens. One Ag-injected GF and one uninjected GF per bird were collected before (0 h), and at 0.1, 0.5, 1, 2, 24, and 48 h post-intravenous injection; organs were collected at 3 d and 7 d post intravenous injection. Tissue sections of the collected GFs and organs were prepared and stained with Prussian blue stain.

Table 1. Experimental procedures to determine iron concentration in plasma, serum and homogenized tissue samples

Experimental procedures	Iron assay kit used
1. Determine iron concentration in IO-plasma samples prepared by adding IO directly to plasma [1]	Sigma Aldrich
2. Determine iron concentration in IO-plasma samples prepared from whole blood spiked directly with IO before plasma preparation blood [2]	Sigma Aldrich
3. Determine iron concentration in plasma samples of IO injected chickens from Experiment 1	Sigma Aldrich
4. Determine iron concentration in IO-serum samples prepared by adding IO directly to serum [1]	Sigma Aldrich
5. Determine iron concentration in IO-serum samples prepared from whole blood spiked directly with IO before coagulation and serum isolation blood [2]	Sigma Aldrich
6. Determine iron concentration in IO-serum samples prepared from whole blood spiked directly with IO before coagulation and serum isolation blood [2]	BioChain
7. Determine iron concentration in serum samples of IO injected chickens from Experiment 2	Sigma Aldrich
8. Determine iron concentration of homogenized tissue samples collected from IO injected chickens from Experiment 2	Sigma Aldrich, BioChain

[1] Two mL of heparinized/non-heparinized whole blood was collected from 9-week-old Light-brown Leghorn female. Blood was spun to get plasma/serum. Plasma/serum was then diluted with PBS at ratio of 1:4. 4.46 µL of 5 mg/mL IO (22.3 µg IO) was added into 995.54 µL of diluted plasma/serum to make 1 mL of IO-added plasma/serum (22.3 µg IO/mL). The IO-added plasma/serum was then serially diluted using doubling dilutions (1/2, 1/4, 1/8, 1/16, 1/32 and 1/64) to yield plasma/serum concentrations of IO of 11.5, 5.575, 2.188, 1.394, 0.697, and 0.348 µg/mL, respectively. No IO was added to the undiluted (0) plasma/serum samples. Iron concentrations of all IO-plasma/IO-serum samples were determined using iron assay kit (Sigma Aldrich).

2) Two mL of heparinized/non-heparinized whole blood was collected from a 9-week-old Light-brown Leghorn female. Forty µL of 5 mg/mL IO was added right away to the blood to make 100 µg/mL IO-added whole blood. The IO-added whole blood was spun to isolate IO-plasma/IO-serum collected. The IO-plasma/IO-serum was then serially diluted with PBS using doubling dilutions (1, 1/2, 1/4, 1/8, 1/16, 1/32 and 1/64) to yield serum concentrations of IO of 100, 50, 25, 12, 6.25, 3.125, and 1.563 µg/mL, respectively. The iron concentrations of all IO-plasma/IO-serum samples were determined using iron assay kit (Sigma Aldrich).

RESULTS

1. Iron Concentration in Plasma, Serum and Homogenized Tissue Samples Collected in Experiment 1 and 2

Heparinized blood or whole blood without an anti-coagulant was centrifuged to collect plasma or serum. Frozen tissues were homogenized and centrifuged to collect supernatant fluid. The iron concentration of plasma, serum, or the supernates were determined using two commercial iron assay kits (Sigma Aldrich kit and BioChain kit). Results were summarized in Table 2.

Iron determination in plasma samples was not successful with the Sigma Aldrich kit. OD values of plasma samples were either outside of the limits of the standard curve (were above the limits and no differences among dilutions), or there were no differences between iron level in plasma samples post IO-injection and 0-time plasma samples (Table 2).

When IO was directly added to serum (IO-added serum) and serial dilutions of the IO-added serum were prepared for analysis, there were not differences in IO concentrations detected using the Sigma Aldrich iron assay kit (Table 2 and Table 3). When IO was added to whole blood, then serum isolated and serially diluted, relative amount of added IO was detected, but concentrations detected in IO-serum samples were much lower than predicted based on IO-added to the whole blood (Table 2 and Table 4). For serum samples prepared from Experiment 2, the standard curve describing the relationship between absorbance unit and iron concentration (nmole), was determined by equation $y = 0.1512x + 0.0047$ with a high R^2 value ($R^2 = 0.99782$) (Figure 2); but iron level in samples post IO injection were not different from 0-time samples. Any effort to determine iron content serum samples with the BioChain kit (Table 2) was unsuccessful.

Iron concentrations of supernatant collected from homogenized PBS- and IO-injected tissue samples were not different (Table 2).

2. Examination of Prussian Blue (Iron Stain) Stained Tissue Sections of Organs Collected from Chickens that were Intravenously Injected with Iron Oxide Nanoparticles

The formalin-fixed tissue samples were paraffin-embedded; sections were prepared and stained with Prussian blue iron stain. Sections were observed under a light microscope system, and pictures were taken at 100 x and 400 x magnification. While lung and kidney showed no iron-stained cells (blue cells) (Figure 3), liver and spleen showed many iron-stain cells in the sections (Figure 4). At 400 x magnification, individual blue cells could be identified in the liver sections; whereas, individual blue cells overlapped in marginal zones of the spleen sections (Figure 5).

2.1. Experiment 1: Dose effect on spleen and liver uptake of i.v. injected IO-COOH

Prussian blue staining in tissue sections were quantified at 400 x magnification by image analysis. For spleens, the relationship between the area of blue staining (% Area) in spleens collected 60-min post-i.v. injection of IO-COOH and the dose of the IO nanoparticles injected was found to be determined by a liner equation y = 1.8578 x – 0.188 with high R^2 value (R^2 = 0.9144), and very low *P*-value (*P* = 0.000202). IO-stained cells (% Area) increased when intravenously injected IO concentration increased, ranging from 3.003 ± 0.211 % Area stained to 8.194 ± 0.915 % Area stained with IO dose of 1.5 and 4.5 mg respectively (Figure 6). For the liver, the relationship was determined by equation y = 0.0785 x + 1.9314 with low R^2 value (R^2 = 0.0466), and no significant relationship between dose of IO injected and blue staining was found

for liver tissue ($P = 0.216$). % Area fluctuated between 1.400 and 2.836 when IO dose increased from 1.5 to 4.5 mg (Figure 6).

2.2. Experiment 2: Comparison of spleen and liver uptake of IO-COOH and IO-PEG administered i.v. at the same dose

Prussian blue staining in liver and spleen tissue sections were quantified at 400 x magnification by two methods including image analysis and manual counting method.

2.2.1. Image analysis method

Compared to uninjected tissues (0.087 ± 0.052), % Area of iron positive staining in spleen sections from IO-COOH injected chickens increased greatly to 3.197 ± 0.496 at 5 min, remained near this level at 15, 30, and 60 min post-injection (to 3.816 ± 0.247, 3.034 ± 0.240 and 3.003 ± 0.211, respectively) (Figure 7). % Area of iron positive staining in liver sections increased within 30 min (from 0.427 ± 0.262 at 0 min to 1.720 ± 0.449 at 30 min), and still remained near this level for 60 min (2.120 ± 0.169) (Figure 7).

In spleens from IO-PEG injected chickens, the % Area of iron positive staining increased very slightly within 15 min (from 0.087 ± 0.052 at 0 min to 0.274 ± 0.065 at 15 min), remained at this level at 30 min (0.217 ± 0.064), and increased further by 60 min (0.517 ± 0.133) (Figure 6). % Area of iron positive staining in liver tissue only marginally increased by 30 min (0.427 ± 0.262 at 0 time to 0.917 ± 0.254), but reached significantly higher levels by 60 min (1.862 ± 0.135) (Figure 7).

Side-by-side comparison of iron staining (% Area) following IO-COOH compared to IO-PEG injection, suggests that uptake of IO-PEG was delayed and lower in both spleen and liver.

By 60 min, the % Area of iron positive staining in the spleen of IO-PEG injected chickens was approximately 8 times lower (0.517 ± 0.133) than in chickens injected with IO-COOH (4.287 ± 0.903) (Figure 7). There were no differences in the % Area of iron positive staining in liver sections from IO-PEG and IO-COOH injected chickens collected 60 min post-injection (1.862 ± 0.135 vs 2.120 ± 0.169, respectively), although % area staining was lower for IO-PEG at earlier time-points. (Figure 7).

2.2.2. Manual counting method

For IO-COOH injection, counting iron stained blue cells in spleen was not determined because individual blue cells overlapped and were not clearly outlined for individual cell counting. However, the number of iron containing liver cells in IO-COOH injected birds could be easily identified and counted. The number of iron positive liver cells (# per 62500 μm^2) in liver sections from IO-COOH injected chickens increased greatly within 5 min (from 6.675 ± 1.676 at 0-time to 33.283 ± 2.887 at 5 min), remained near this level for 30 minutes, then increased further (34.983 ± 3.020 at 30 min to 46.867 ± 1.048 at 60 min) (Figure 8).

For IO-PEG injection, the number of iron positive spleen cells increased greatly within 5 minutes post-injection (from 0.050 ± 0.050 pre-injection to 1.483 ± 0.233 at 5 min), increased further to 2.383 ± 0.913 at 15 minutes, remained near this level at 30 min (1.850 ± 1.050) and increased again to 8.383 ± 0.017 by 60 min (Figure 8). Compared to the number of blue-stained cells in livers collected before IO-PEG injection (6.675 ± 1.676), the number of iron-containing cells in livers from chickens injected with IO-PEG did not increase until 30 min (17.250 ± 7.556), and this level was not different from the number of iron-positive cells at 60 min (33.633 ± 11.181) (Figure 8).

With this Counting method, the number of iron positive liver cells in IO-PEG injection also was lower than number of iron positive liver cells following i.v. injection of IO-COOH nanoparticles (Figure 8).

In addition, the comparison of data obtained using image analysis (% Area) and manual counting (cells/62500 μm^2) was analyzed by Pearson Correlation Test (Figure 9). For spleens from IO-PEG injected birds the correlation between the iron staining data obtained using the two different methods was determined by a liner equation y = 12.563x − 0.1342 with R^2 = 0.6696, and very low *P*-value (*P* = 0.000182). Similarly, for livers from IO-PEG injected chickens, the correlation between iron staining data obtained using the two methods was determined by a liner equation y = 16.925x + 1.7456 with R^2 = 0.6422, and very low *P*-value (*P* = 0.000190). For livers from chickens injected with IO-COOH, the correlation between iron staining data obtained using the two methods was determined by a liner equation y = 18.93x + 9.1857 with R^2 = 0.6614, and very low *P*-value (*P* = 0.000128). Using iron staining data for livers from all iron oxide nanoparticle injected chickens, (i.e. injected with wither IO-COOH or IO-PEG), the correlation between the data obtained using the two different methods was determined by a liner equation y = 19.908x + 4.0876 with R^2 = 0.64, and very low *P*-value (*P* = 0.000000324). (Figure 9).

3. Iron Staining for Frozen Tissues using Peroxidase Mimicking Activity of Iron Oxide Nanoparticles

Frozen tissue sections were prepared and incubated in H_2O_2 and DAB, respectively. Iron positive cells (brown color cells) were determined at 400 x magnification. As expected, there were no brown cells in lung and kidney. In liver sections of IO-COOH injected chickens, many

iron positive (brown) cells, similar in location and appearance to those observed in fixed Prussian blue stained liver sections could be observed (Figure 10a and Figure 5b). There were many brown particles in the cytoplasm of the liver cells (Figure 10a). There were no brown cells in liver sections of PBS injected chickens (Figure 10b). Conducting iron staining using the peroxidase mimicking activity of iron oxide nanoparticles was not successful for spleen sections, where due to high background staining, individual iron containing cells could not be identified (data not shown).

4. Immunohistochemical and Prussian Blue Staining (HT20 kit) of Frozen Tissues Sections

Liver and spleen frozen sections were stained by combinations of variations of immunohistochemical and Prussian blue staining. Formalin fixing (0 min, 20 min, overnight) was combined with staining by the HT20 working solution (10 min, overnight). The results were described in Table 5. Specifically, for liver sections, the combination of 20 min formalin fixing and overnight staining in HT20 working solution resulted in the most effective (+++++) iron staining. The combination of no formalin fixing and 10 min staining with the HT20 working solution was the least effective iron-staining (+). The other combination showed intermediate effective iron staining (levels at ++ or +++; Table 5). After optimizing dual immunostaining for leukocyte markers and iron staining with the HT20 kit, examination of dual stained liver sections from IO-COOH injected chickens confirmed that the iron-stain (blue color) was located in macrophages and MHC-II positive cells (brown color) (Figure 11 and Figure 12). Tissue sections stained using the isotype control antibodies in combination with iron-staining revealed only iron-containing blue cells, and no brown staining, confirming that there was no non-specific binding

of the cell-specific antibodies used to identify macrophages, MHC-II+ cells, and B cells (all mouse IgG1 monoclonal antibodies) (Figure 13).

For spleen, iron-staining of frozen tissue section using the HT20 kit was most effective using a combination of no formalin fixing and overnight incubation in HT20 working solution (++++). The other combinations tested were much less effective (+, ++) (Table 5). For spleen sections from IO-COOH injected chickens, iron-stain (blue color) was also located in what appeared to be marginal zone, MHC-II positive macrophages (brown color) (Figure 14 and Figure 15), but not in B cells (Bu-1$^+$) that are also known to be MHC-II positive (Figure 16). It should be noted that for the spleen the immunohistochemical staining for macrophages in combination with Prussian blue staining was not clearly interpretable as the cells stained very red (Figure 14) instead of showing clear brown and blue staining. However, based on location, H/E staining, individual iron or KUL-01 staining, and MHC class II staining, the iron stained cells in the spleen appear to be macrophages. Spleen tissue sections stained using the isotype control antibodies in combination with iron-staining revealed only iron-containing blue cells, and no brown staining, confirming that there was no non-specific binding of the cell-specific antibodies used to identify macrophages, MHC-II+ cells, and B cells (all mouse IgG1 monoclonal antibodies) (Figure 17).

5. Experiment 3: Iron Oxide Nanoparticle Delivery/Targeting Study

Microscopic evaluation of Prussian blue stained sections prepared from formalin fixed growing feathers (GFs) that were intradermally injected with mouse IgG antigen 6 hours before intravenous injection of iron oxide nanoparticles, revealed no accumulation of iron in the dermis

of mouse IgG injected GFs at any of the time time-points examined (before and at 0.1, 0.5, 1, 2, 24 and 48 h post i.v. injection of IO nanoparticles). Although, based on H/E staining of GFs, mouse IgG induced leukocyte recruitment to the dermis in injected GFs, a process that was indicative of vascular changes that should allow nanoparticles to leave the blood and enter the inflamed tissue. The lack of iron staining in the GF tissue sections was independent of the type of IO nanoparticle injected i.v.; i.e. IO-conjugated with chicken anti-mouse IgG antibody, IO-COOH or IO-PEG. Iron staining of spleens and livers collected from the chickens 3 or 7 days post-i.v. injection of IO nanoparticles revealed presence of iron staining in the marginal zone areas of the spleen as well as in liver cells (data not shown).

Table 2. Iron concentration in plasma, serum, and homogenized tissue samples

Samples	Iron assay kit used	Concentration of iron determined
1. IO-plasma samples prepared by adding IO-NP directly to plasma [1]	Sigma Aldrich	OD values were out of the standard curve, plasma may affect the OD values
2. IO-plasma samples prepared from whole blood spiked directly with IO-NP before plasma preparation [2]	Sigma Aldrich	OD values were out of the standard curve, plasma may affect the OD values
3. Plasma samples of IO-NP injected chickens from Experiment 1	Sigma Aldrich	Iron level in samples post IO-NP injection were not different from 0-time samples
4. IO-serum samples prepared by adding IO-NP directly to serum [1]	Sigma Aldrich	The added IO-NP was not detected and no dilution curve (Table 3)
5. IO-serum samples prepared from whole blood spiked directly with IO-NP before coagulation and serum isolation [2]	Sigma Aldrich	Relative amount of added IO-NP was detected but at very low levels (Table 4)
6. IO-serum samples prepared from whole blood spiked directly with IO-NP before coagulation and serum isolation blood [2]	BioChain	Not detected
7. Serum samples of IO-NP injected chickens from Experiment 2	Sigma Aldrich	Standard curve worked well (Figure 2), iron level in samples post IO-NP injection were not different from 0-time samples
8. Homogenized tissue samples collected from IO-NP injected chickens from Experiment 2	Sigma Aldrich, BioChain	Iron concentrations of PBS and injected samples were not different

[1] Two mL of heparinized/non-heparinized whole blood was collected from a 9-week-old Light-brown Leghorn female. Blood was spun to get plasma/serum. Plasma/serum was then diluted with PBS at ratio of 1:4. 4.46 µL of 5 mg/mL IO-COOH (22.3 µg IO) was added into 995.54 µL of diluted plasma/serum to make 1 mL of IO-added plasma/serum (22.3 µg IO/mL). The IO-added plasma/serum was then serially diluted using doubling dilutions (1/2, 1/4, 1/8, 1/16, 1/32 and 1/64) to yield plasma/serum concentrations of IO of 11.5, 5.575, 2.188, 1.394, 0.697, and

0.348 µg/mL, respectively. No IO nanoparticles (NP) were added to the undiluted (0) serum samples. IO concentration of all IO-plasma/IO-serum samples were determined using iron assay kit (Sigma Aldrich).

[2)] Two mL of heparinized/non-heparinized whole blood was collected from a 9-week-old Light-brown Leghorn female. Forty µL of 5 mg/mL IO-COOH was added right away to the blood to make 100 µg/mL IO-added whole blood. The IO-added whole blood was spun to isolate IO-plasma/IO-serum collected. The IO-plasma/IO-serum was then serially diluted with PBS using doubling dilutions (1, 1/2, 1/4, 1/8, 1/16, 1/32 and 1/64) to yield serum concentrations of IO-NP of 100, 50, 25, 12, 6.25, 3.125, and 1.563 µg/mL, respectively. IO concentration of all IO-plasma/IO-serum samples were determined using iron assay kit (Sigma Aldrich).

Table 3. Concentration of iron detected in serum samples to which IO nanoparticles were added prior to serial dilution (IO-added serum) [1]

IO-serum samples	Known concentration of IO in IO-serum samples C (µg/mL)	Concentration of IO detected by using iron assay kit C (µg/mL)
0	0.174	1.225
1/64	0.348	1.370
1/32	0.697	1.291
1/16	1.394	1.350
1/8	2.788	1.330
1/4	5.575	1.416
1/2	11.15	1.370

[1] Two mL of blood was collected from a 9-week-old Light-brown Leghorn female. Blood was allowed to coagulate, samples were centrifuged, and serum collected. Serum was then diluted with PBS at ratio of 1:4. 4.46 µL of 5 mg/mL IO-COOH nanoparticles (22.3 µg IO) was added into 995 µL of diluted serum to make 1 mL of IO-added serum (22.3 µg IO/mL). The IO-added serum was then serially diluted using doubling dilutions (1/2, 1/4, 1/8, 1/16, 1/32 and 1/64) to yield serum concentrations of IO of 11.5, 5.575, 2.188, 1.394, 0.697, and 0.348 µg/mL, respectively. No IO was added to the undiluted (0) serum samples. IO concentration of all IO-serum samples were determined using iron assay kit (Sigma Aldrich).

Table 4. Concentration of iron detected in serum samples prepared from whole blood to which a known amount of IO nanoparticles was added prior to serum isolation[1]

| IO-serum samples	Known concentration of IO-NP in IO-serum samples C (μg/mL)	Concentration of IO detected by using iron assay kit C (μg/mL)
1/64	1.563	0.002
1/32	3.125	0.068
1/16	6.25	0.260
1/8	12.5	0.577
1/4	25	0.815
1/2	50	1.145
1	100	1.787

[1] Two mL of whole blood was collected from a 9-week-old Light-brown Leghorn female. Forty μL of 5 mg/mL IO-COOH was added right away to the blood to make 100 μg/mL IO-added whole blood. The IO-added whole blood was allowed to coagulate, samples were centrifuged, and IO-serum collected. The IO-serum was then serially diluted with PBS using doubling dilutions (1, 1/2, 1/4, 1/8, 1/16, 1/32 and 1/64) to yield serum iron concentrations of of 100, 50, 25, 12, 6.25, 3.125, and 1.563 μg/mL, respectively. IO concentration of all IO-serum samples were determined using iron assay kit (Sigma Aldrich).
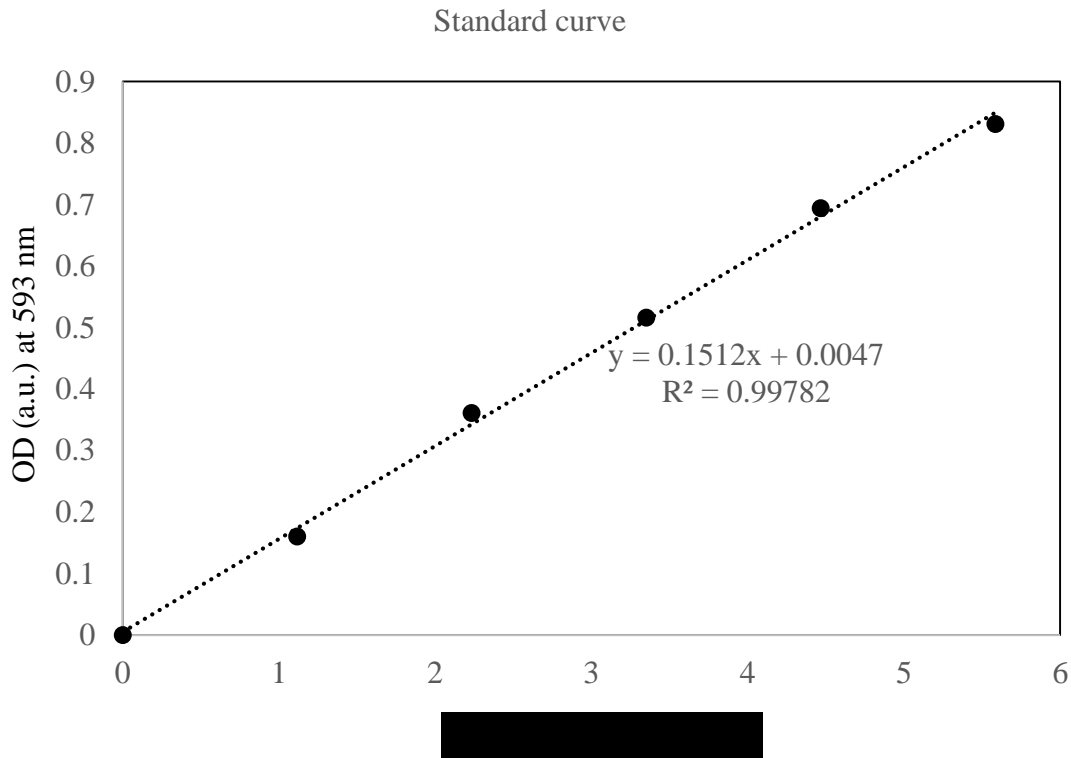
Figure 2. Standard curve obtained for the Sigma-Aldrich iron assay test kit. The 1 mM standard solution was generated by diluting 10 μL of the 100 mM iron standard with 990 μL of distilled water. 0, 2, 4, 6, 8, and 10 μL of the 1 mM standard solution were added into wells of a 96 well plate to generate 0, 2, 4, 6, and 10 nmole/well iron standards, respectively. The iron assay buffer was then added to these wells to bring the volume to 100 μL. Five μL of iron reducer was then added to each of the wells containing standard amounts of iron. The final concentration of standards were 0, 1.117, 2.234, 3.351, 4.468, and 5.585 μg/mL, respectively. The plate was incubated for 30 min at room temperature. After incubation, 100 μL of the iron probe was added to each of well. The plate was incubated for 60 min at room temperature, and color development (optical density; OD) was measured at 593 nm wave length. The OD values were recorded and analyzed using Microsoft Excel software.
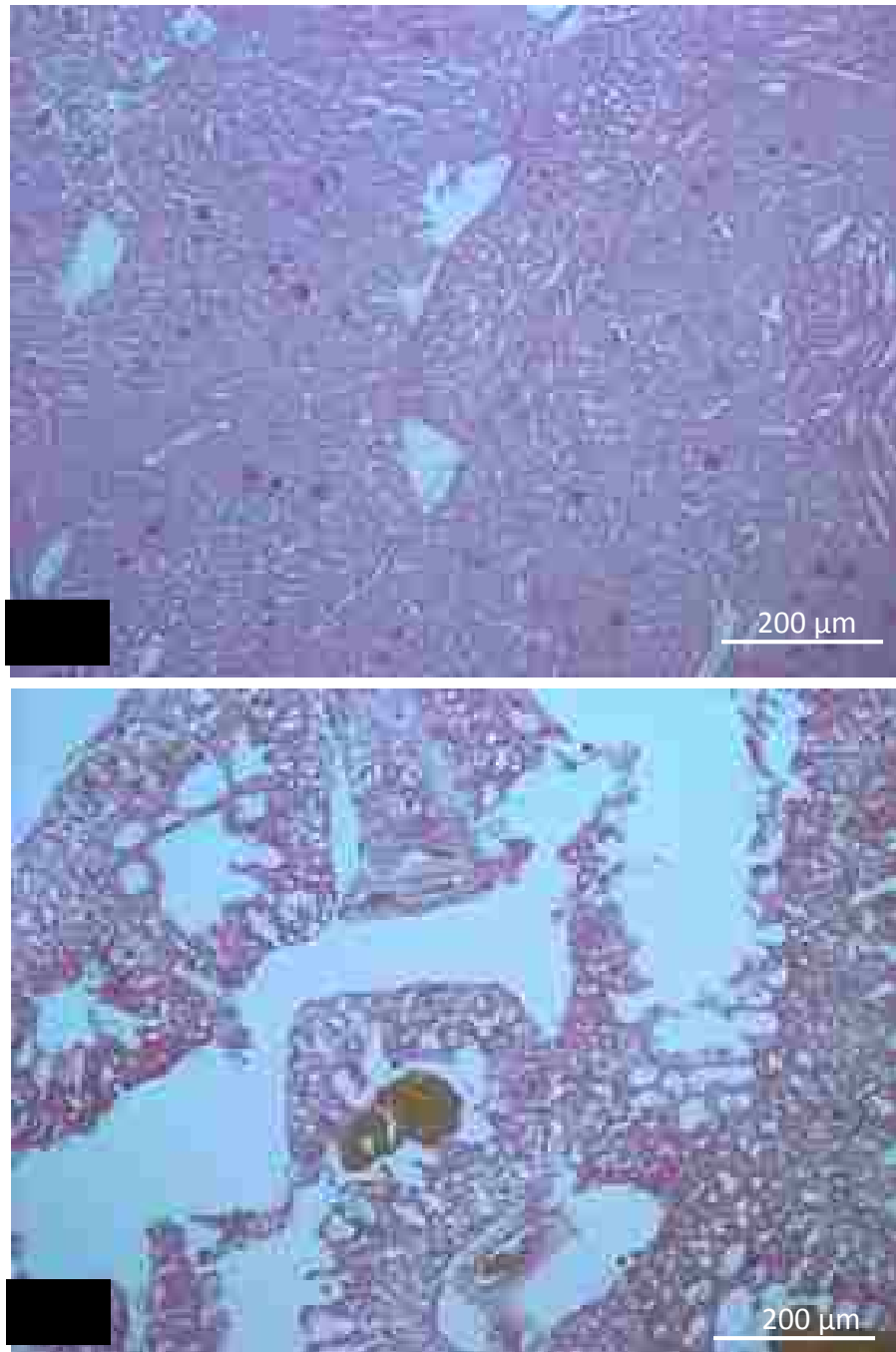
Figure 3. Prussian blue stained kidney (a) and lung (b) tissue sections collected from chickens that were intravenously injected with iron oxide (IO) nanoparticles. Nine-week-old Light-brown Leghorn females were intravenously injected with IO-COOH nanoparticles (dose of 3.3 mg/kg). Chickens were euthanized at 60 min post intravenous injection by injection of pentobarbital solution and the organs were removed. Tissues were formalin-fixed, paraffin-embedded; sectioned (5 µm), and sections stained with Prussian blue stain. Pictures were taken at 400 x magnification using an Olympus BX50 light microscope equipped with a CoolSNAP Pro digital camera.
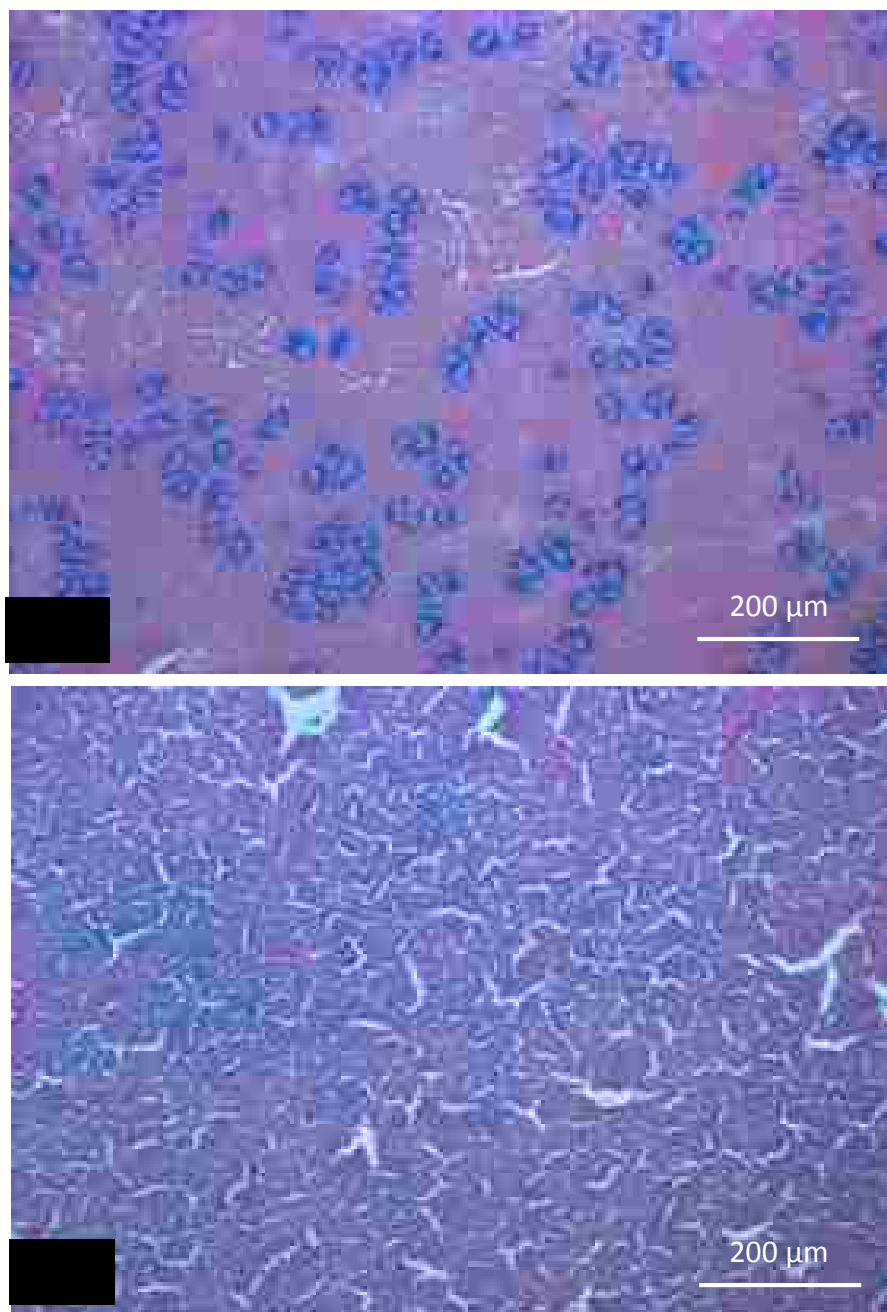
Figure 4. Prussian blue stained spleen (a) and liver (b) tissue sections collected from chickens that were intravenously injected with iron oxide nanoparticles. Nine-week-old Light-brown Leghorn females were intravenously injected with IO-COOH nanoparticles (dose of 3.3 mg/kg). Chickens were euthanized at 60 min post intravenous injection by injection of pentobarbital solution and the organs were removed. Tissues were formalin-fixed, paraffin-embedded; sections (5 µm) were prepared and stained with Prussian blue iron stain (blue cells). Pictures were taken at 100 x magnification using an Olympus BX50 light microscope equipped with a CoolSNAP Pro digital camera.
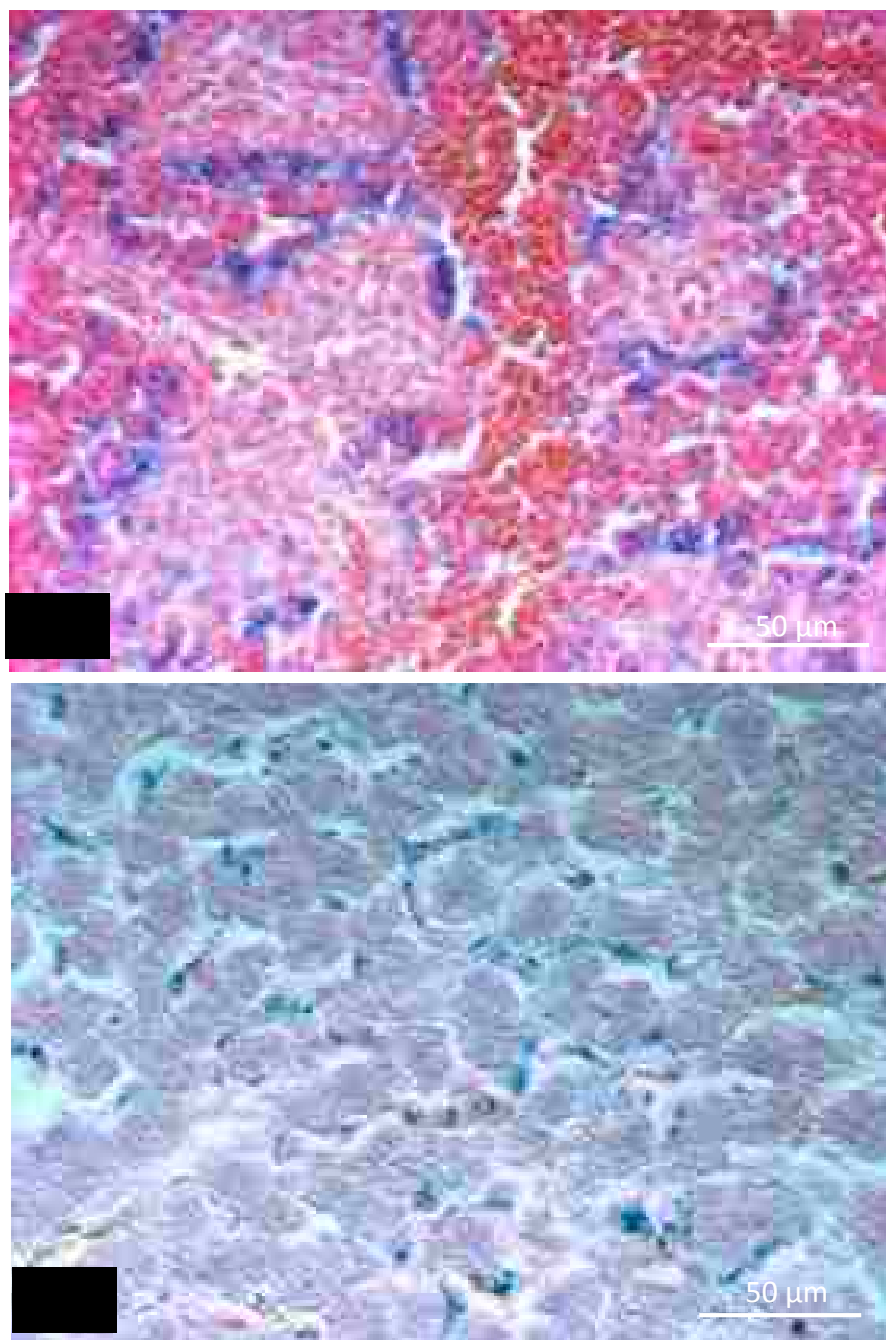
Figure 5. Prussian blue stained spleen (a) and liver (b) tissue sections collected from chickens that were intravenously injected with iron oxide (IO) nanoparticles. Nine-week-old Light-brown Leghorn females were intravenously injected with IO-COOH nanoparticles (dose of 3.3 mg/kg). Chickens were euthanized at 60 min post intravenous injection by injection of pentobarbital solution and the organs were removed. Tissues were formalin-fixed, paraffin-embedded; sectioned (5 μm) and sections stained with Prussian blue iron stain (blue cells). Pictures were taken at 400 x magnification using an Olympus BX50 light microscope equipped with a CoolSNAP Pro digital camera.
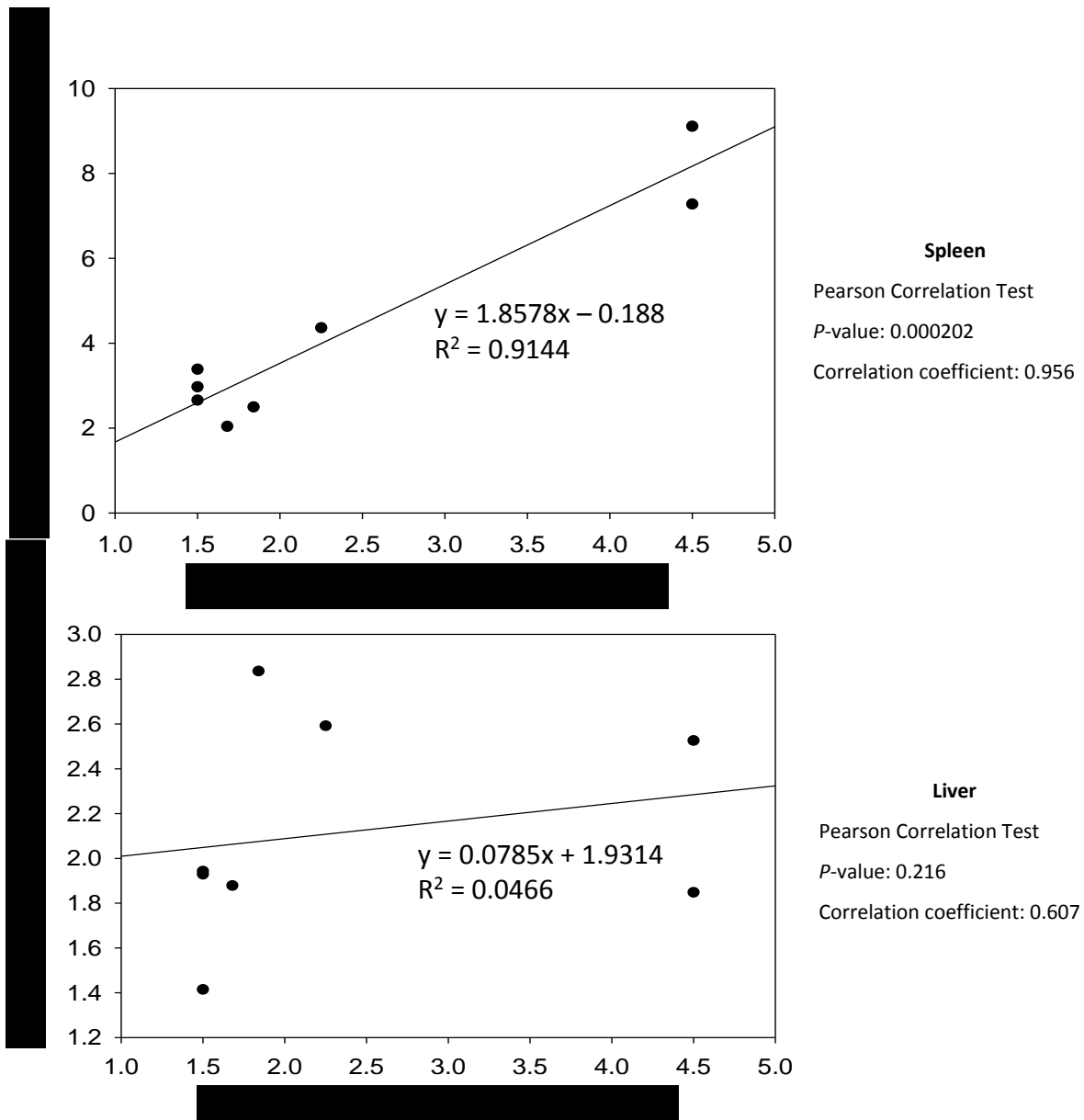
Spleen

Pearson Correlation Test

P-value: 0.000202

Correlation coefficient: 0.956

$$y = 1.8578x - 0.188$$
$$R^2 = 0.9144$$

Liver

Pearson Correlation Test

P-value: 0.216

Correlation coefficient: 0.607

$$y = 0.0785x + 1.9314$$
$$R^2 = 0.0466$$

Figure 6. Relationship between percentage of iron-stained cells in spleen and liver of chickens injected intravenously with iron oxide nanoparticles. Nine-week-old Light-brown Leghorn females were intravenously injected with various doses of IO-COOH (IO) nanoparticles (1.5, 1.68, 1.84, 2.25, or 4.5 mg) or PBS. Chickens were euthanized at 60 min post intravenous injection by injection of pentobarbital solution and the organs were removed. Tissues were formalin-fixed, paraffin-embedded; sectioned (5 μm) and sections stained with Prussian blue iron stain. Blue staining in sections was quantified as % Area (blue area/field; 20 fields per section) by image analysis (Image Pro software) at 400 x magnification using an Olympus BX50 light microscope equipped with a CoolSNAP Pro digital camera, and computer connection. Data were analyzed using Pearson Correlation Test, Sigma Plot 13 Statistical Software. For spleen, *P*-value was 0.000202, correlation coefficient was 0.956. For liver, *P*-value was 0.216, and correlation coefficient was 0.607.
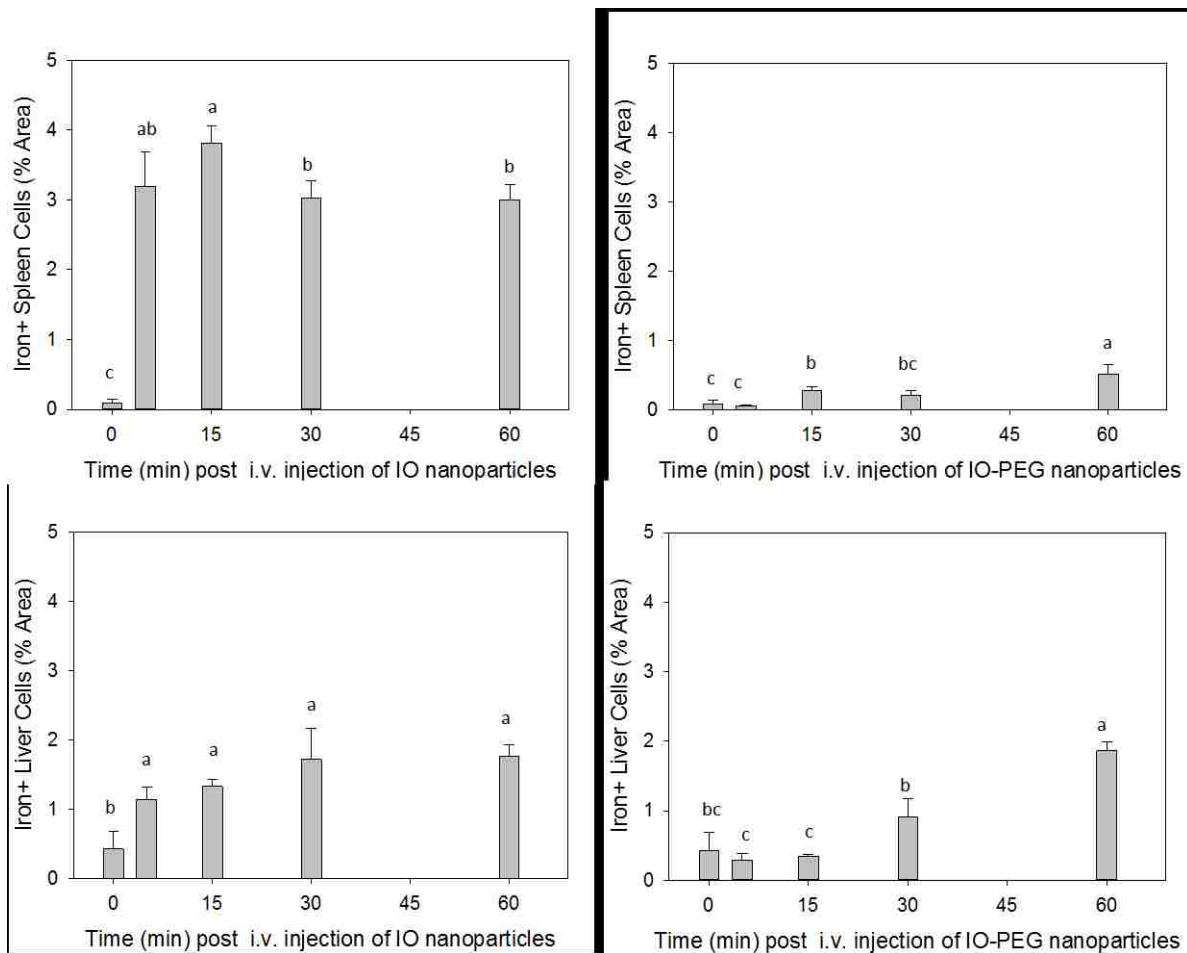
Figure 7. Extent (% Area) of iron positive staining in spleen and liver sections at various time points post intravenous injection of iron oxide nanoparticles. Nine-week-old Light-brown Leghorn females were intravenously injected with IO-COOH (IO) or IO-PEG nanoparticles (dose of 3.3 mg/kg). Chickens were euthanized at 0, 5, 15, 30, and 60 min post intravenous injection by injection of pentobarbital solution and the organs were removed. Tissues were formalin-fixed, paraffin-embedded; sectioned (5 µm), and sections stained with Prussian blue iron stain. Blue staining in spleen and liver sections was quantified as % Area (blue area/field, 20 fields per section) by image analysis (Image Pro software) at 400x magnification using an Olympus BX50 light microscope equipped with a CoolSNAP Pro digital camera, and computer connection. Data shown are mean ± SEM (n=3 for IO or IO-PEG injection per time-point, and n=4 for PBS injection). Following one-way ANOVA, Fisher's LSD multiple means comparison test was used to determine differences between time-points. a-c: means without a common letter is different ($P < 0.05$).
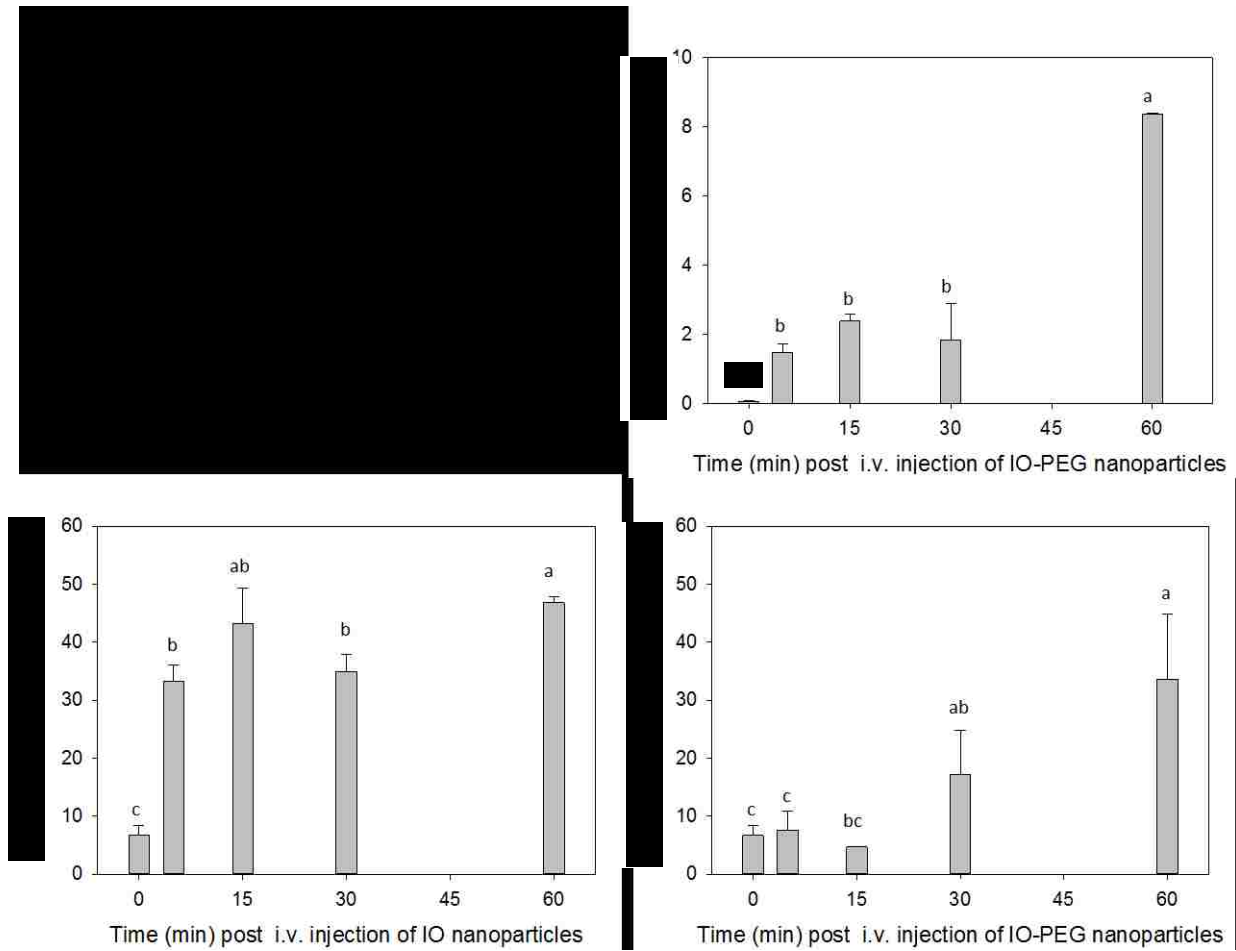
Figure 8. Number of iron positive cells per 62500 μm^2 tissue area in spleen and liver of chickens that were intravenously injected with iron oxide nanoparticles. Nine-week-old Light-brown Leghorn females were intravenously injected with IO-COOH (IO) or IO-PEG nanoparticles (dose of 3.3 mg/kg) and PBS. Chickens were euthanized at 0, 5, 15, 30, and 60 min post intravenous injection by injection of pentobarbital solution and the organs were removed. Tissues were formalin-fixed, paraffin-embedded; sectioned (5 μm), and sections stained with Prussian blue iron stain. Stained sections were examined by bright-field microscopy and cells quantified by counting the number of blue cells per 62500 μm^2 (#62500 μm^2) at 400 x magnification with the aid of an ocular grid insert (10 mm x 10 mm). Sections were scanned to confirm IO nanoparticle presence (blue cells), and number of blue stained cells counted in 20 areas (62500 μm^2/area). Data shown are mean ± SEM (n=3 for IO-COOH or IO-PEG injection, and n=4 for PBS injection). Following one-way ANOVA, Fisher's LSD multiple means comparison test was used to determine differences between time-points. a-c: means without a common letter are different (P <0.05).
Note: Counting blue cells in spleen from IO-injected birds was not reliable because individual blue cells overlapped and were not as clearly outlined as in the liver.

48
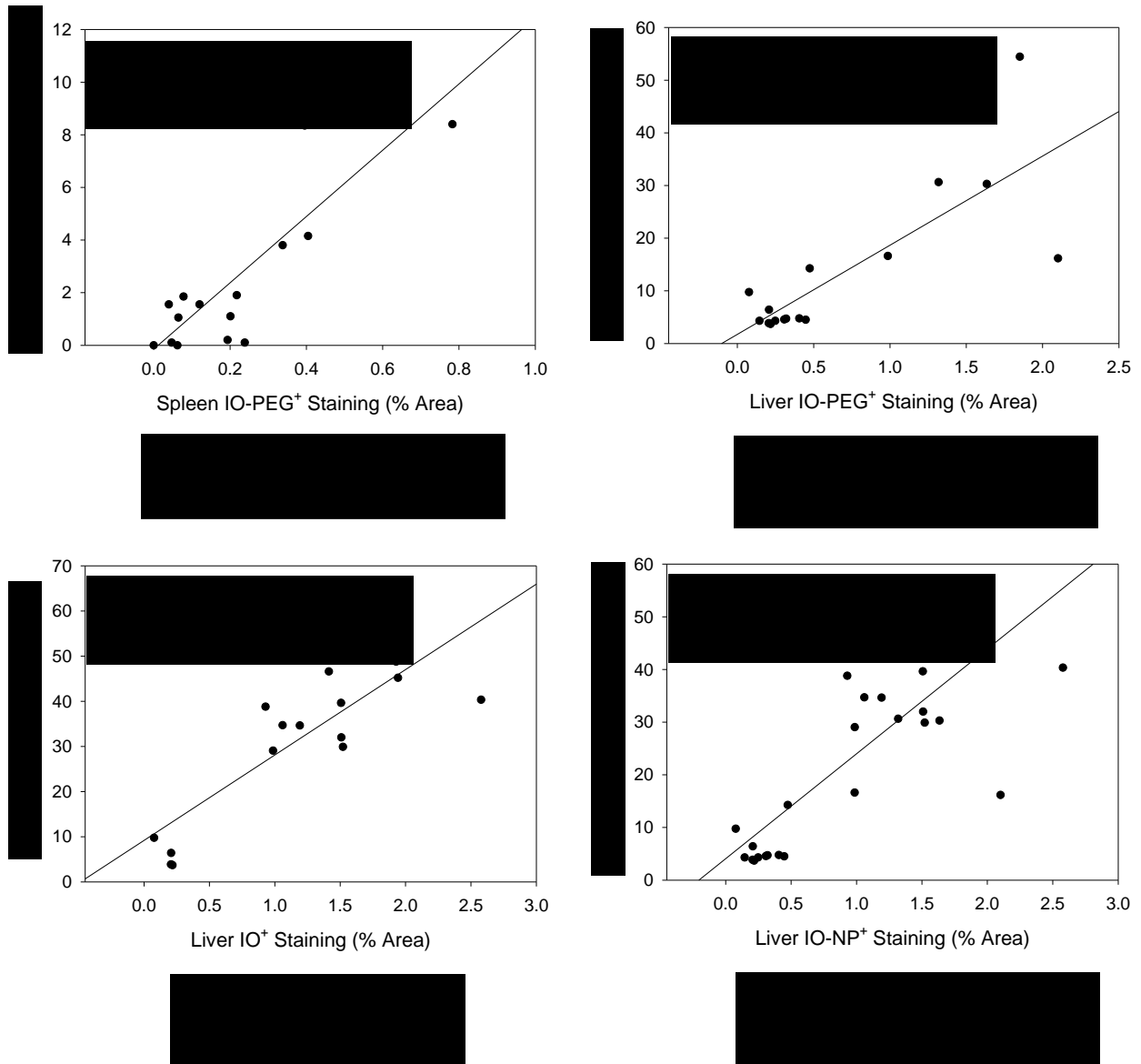
Figure 9. Comparison between image analysis and manual count. Nine-week-old Light-brown Leghorn females were intravenously injected with IO-COOH (IO) or IO-PEG nanoparticles (dose of 3.3 mg/kg) and PBS. Chickens were euthanized at 0, 5, 15, 30, and 60 min post intravenous injection, and the organs were removed. Tissues were formalin-fixed, paraffin-embedded; sectioned (5 μm), and sections stained with Prussian blue iron stain. Stained sections were examined by image analysis and a manual counting method at 400 x magnification. For Image analysis, blue staining was quantified as % Area (blue area/field, 20 fields per section) using Image Pro software and a light microscope equipped with a CoolSNAP Pro digital camera. For the manual count, the number of blue cells per 62500 μm^2 (#62500 μm^2/field, 20 fields per section) were counted using a bright-field microscopy with the aid of an ocular grid insert (10 mm x 10 mm). Data were analyzed using Pearson Correlation Test, Sigma Plot 13 Statistical Software. *P*-values of ≤0.05 are considered significant.
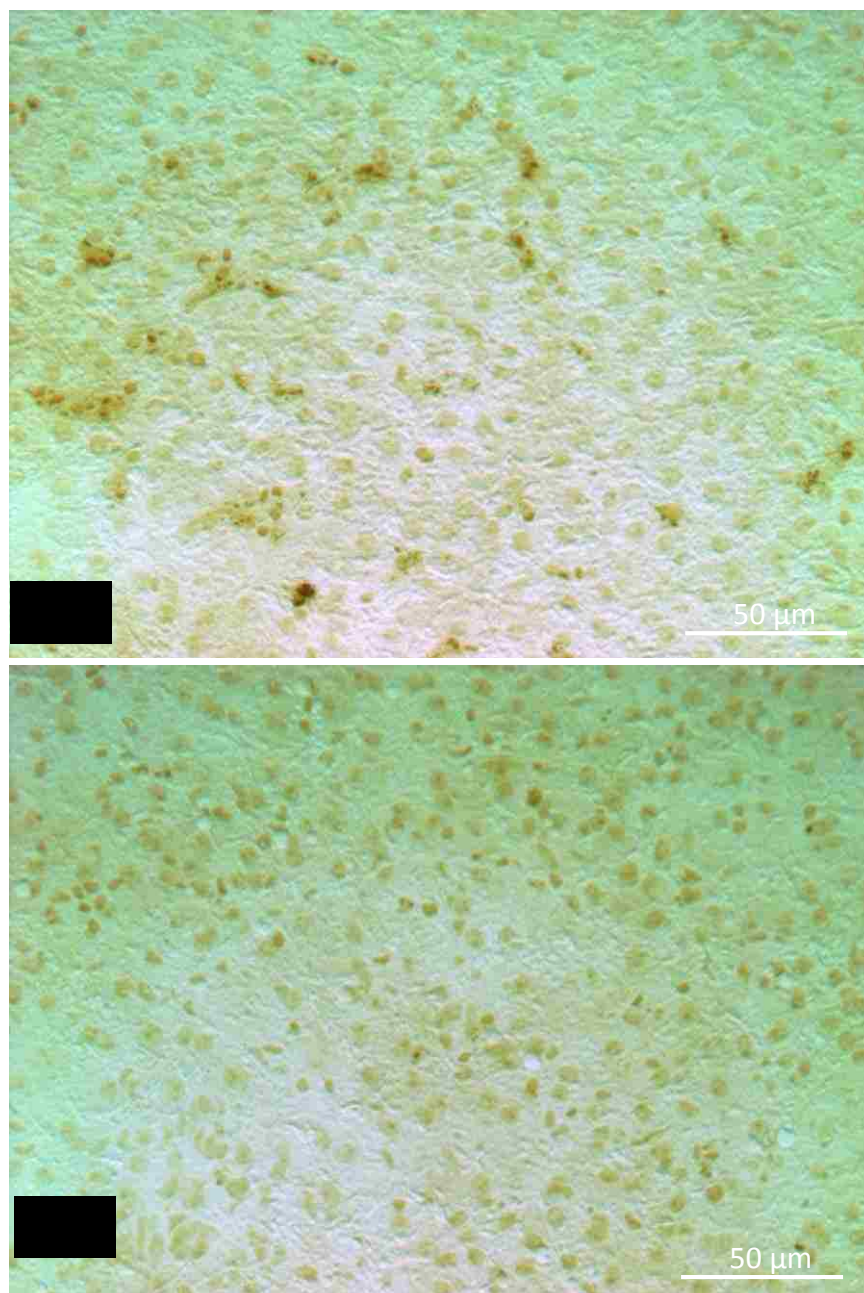
Figure 10. Identification of iron nanoparticle presence in cells of frozen liver tissue sections using the peroxidase mimicking activity of iron oxide (IO) nanoparticles. **(a)** IO injected **(b)** PBS. Nine-week-old Light-brown Leghorn females were intravenously injected with IO-COOH nanoparticles (dose of 3.3 mg/kg) or PBS. The sample sections shown were prepared from livers collected 30 min post intravenous IO/PBS injection. The 7 μm frozen sections were prepared using a cryostat. The sections were incubated in 10% H_2O_2 in methanol for 20 min, and in DAB substrate solution overnight. The slides were washed with PBS, sections covered with Aqua-Mount mounting medium and a glass coverslip. Sections were scanned to confirm iron oxide nanoparticle presence (brown cells), and pictures were taken at 400 x magnification using a light microscope system.

Table 5. Combinations of immunohistochemical (brown stain) and Prussian blue iron staining (HT20 kit) methods tested to optimize dual staining for frozen tissue sections [1]

Combinations	Time fixed in formalin (min)	Time incubated in HT20 working solution (min)	Blue color in brown cells (L: liver, S: spleen) (+: effective level)
1	0	10	L: + S: +
2	0	overnight	L: + + + S: + + + +
3	20	10	L: + + + S: +
4	20	overnight	L: + + + + + S: + +
5	overnight	10	L: + + + S: +
6	overnight	overnight	L: + + + S: +

[1] Nine-week-old Light-brown Leghorn females were intravenously injected with IO-COOH nanoparticles (dose of 3.3 mg/kg). Organs were collected 60 min post intravenous injection, snap frozen with liquid nitrogen. Frozen sections of liver and spleen were prepared and all the steps of immmunohistochemical staining were carried including the DAB incubation step. The sections were then fixed in buffered formalin solution for different lengths of time (0 min - no formalin fixation, 20 min, and overnight). After that, the sections were incubated in HT20 working solution (mixing of Potassium Ferrocyanide Solution and Hydrochloric Acid Solution) for 2 different time-points (10 min and overnight), and were then counterstained with Pararosaniline, washed with PBS, dehydrated, and covered with a glass coverslip.
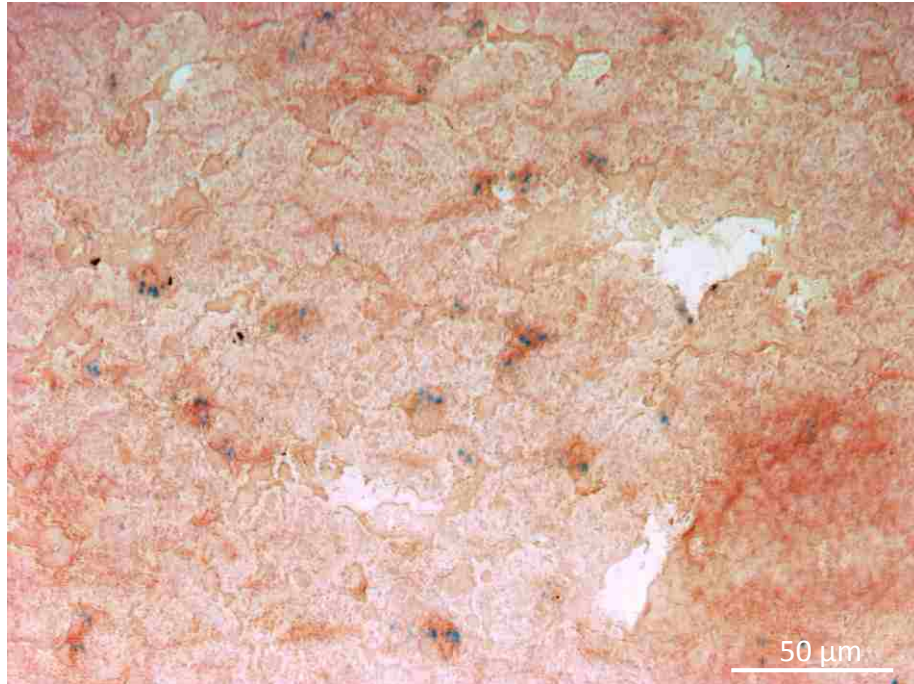
Figure 11. Iron and macrophage double staining in frozen liver tissue sections from chickens injected intravenously with iron oxide (IO) nanoparticles. A 9-week-old Light-brown Leghorn female was intravenously injected with IO-COOH nanoparticles (dose of 3.3 mg/kg). Organs were collected 60 min post-intravenous injection. Frozen liver sections (7 μm) were prepared and stained using indirect immunohistochemistry with chicken macrophage specific antibody (KUL-01) in combination with Prussian blue staining. Sections were scanned to confirm iron positive cells (blue) which were also positive for the macrophage marker (brown). Pictures were taken at 400 x magnification using a light microscope equipped with a digital camera.

Figure 12. Iron oxide and MHC class II double staining in frozen liver tissue sections from chickens injected intravenously with iron oxide nanoparticles. A 9-week-old Light-brown Leghorn female was intravenously injected with IO-COOH nanoparticles (dose of 3.3 mg/kg. Organs were collected 60 min post-intravenous injection. Frozen liver sections (7 µm) were prepared and stained using indirect immunohistochemistry with chicken MHC class II specific antibody in combination with Prussian blue staining. Sections were scanned to confirm iron positive cells (blue) which were also positive for the MHC class II marker (brown). Pictures were taken at 400 x magnification using a light microscope equipped with a digital camera.

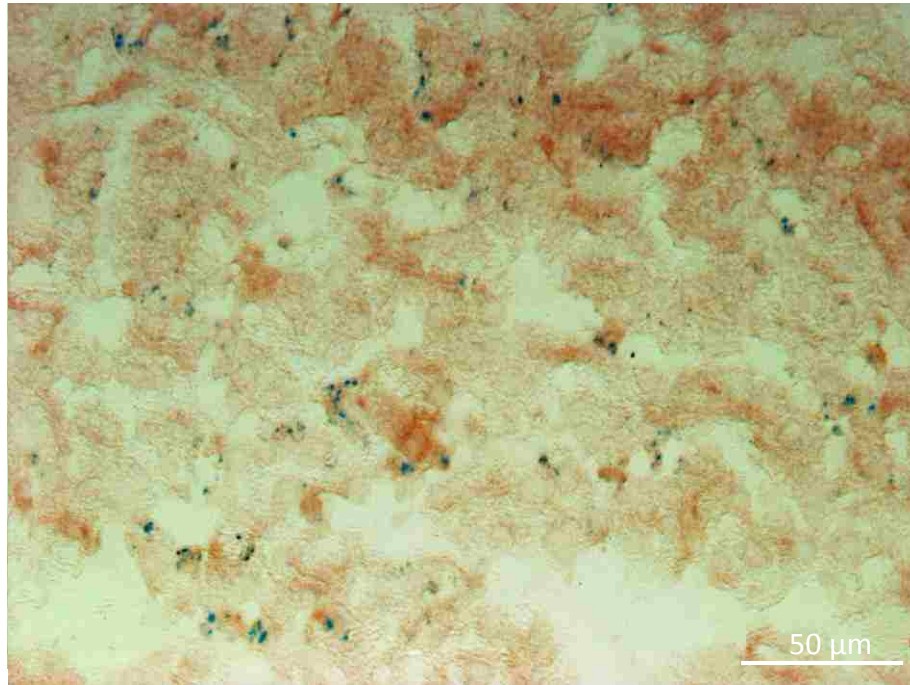**Figure 13.** Iron oxide and isotype control double staining in frozen liver tissue sections from chickens injected intravenously with iron oxide nanoparticles. A 9-week-old Light-brown Leghorn female was intravenously injected with IO-COOH nanoparticles (dose of 3.3 mg/kg). Organs were collected 60 min post-intravenous injection. Frozen liver sections (7 µm) were prepared and stained using indirect immunohistochemistry with isotype control (mouse IgG1) antibodies in combination with Prussian blue staining. Sections were scanned to confirm iron positive cells and absence of non-specific binding of the cell-specific antibodies (all IgG1) used to identify macrophages, MHC-II+ cells, and B cells (no brown staining). Pictures were taken at 400 x magnification using a light microscope equipped with a digital camera.
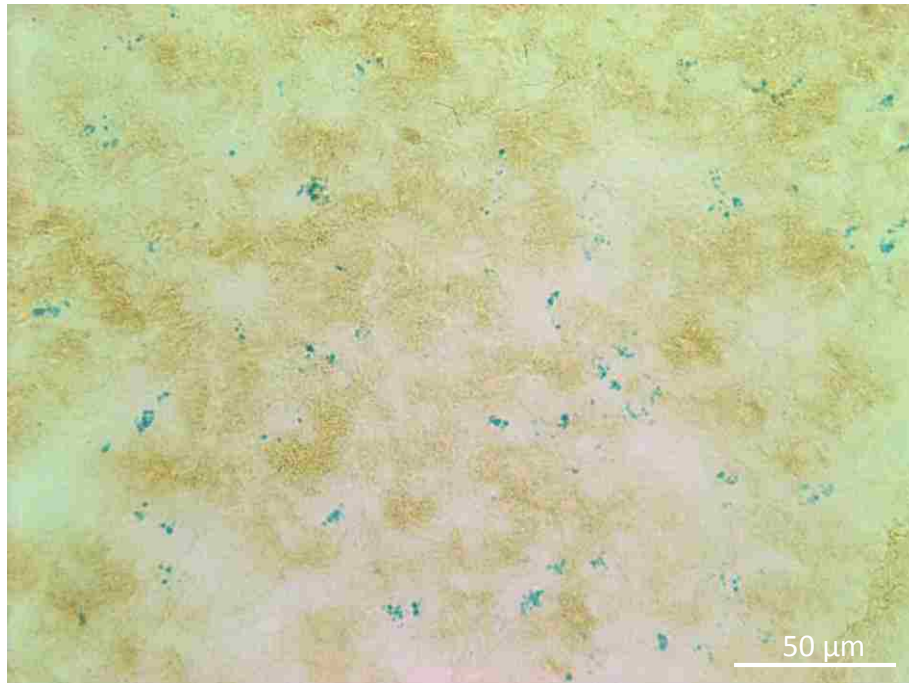
Figure 14. Iron oxide and macrophage double staining in frozen spleen tissue sections from chickens injected intravenously with iron oxide nanoparticles. A 9-week-old Light-brown Leghorn female was intravenously injected with IO-COOH nanoparticles (dose of 3.3 mg/kg). Organs were collected 60 min post-intravenous injection. Frozen spleen sections (7 µm) were prepared and stained using indirect immunohistochemistry with chicken macrophage specific antibody (KUL-01) in combination with Prussian blue staining. Double staining was not clearly interpretable with spleen sections. Pictures were taken at 400 x magnification using a light microscope equipped with a digital camera.
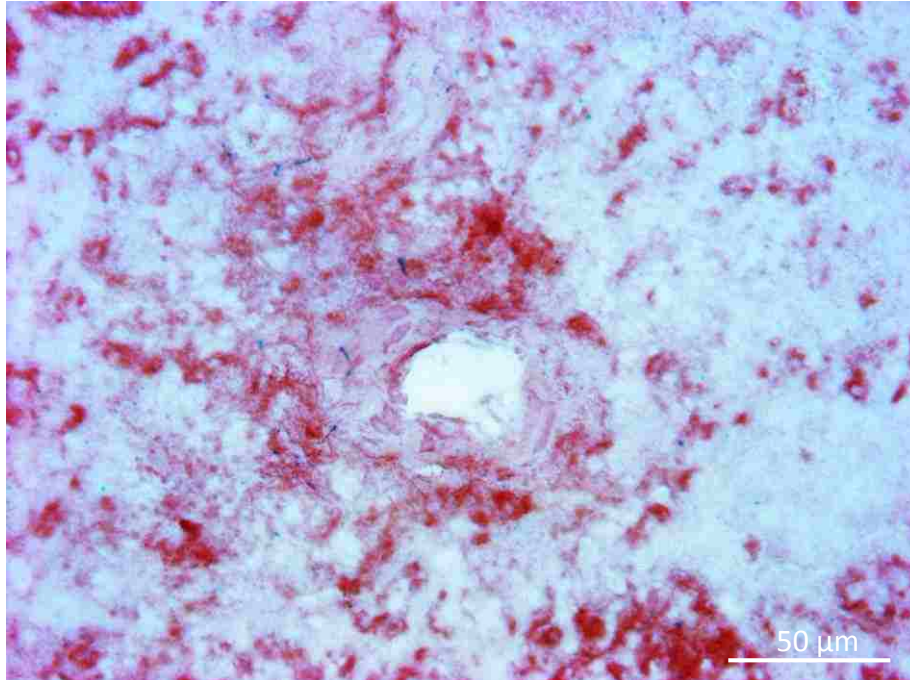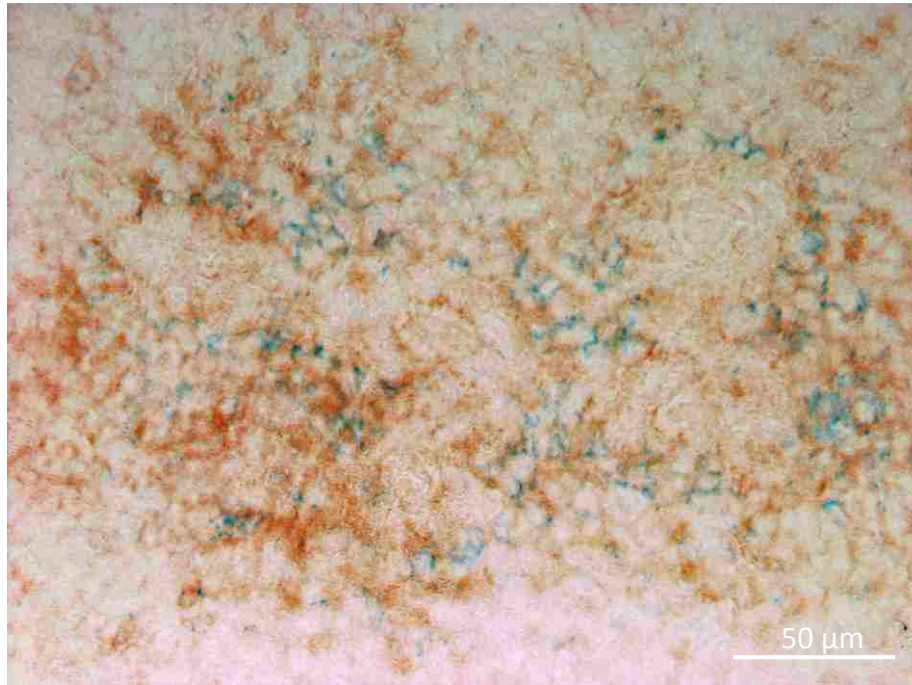
Figure 15. Iron oxide and MHC class II double staining in frozen spleen tissue sections from chickens injected intravenously with iron oxide nanoparticles. A 9-week-old Light-brown Leghorn female was intravenously injected with IO-COOH nanoparticles (dose of 3.3 mg/kg). Organs were collected 60 min post-intravenous injection. Frozen spleen sections (7 μm) were prepared and stained using indirect immunohistochemistry with chicken MHC class II specific antibody in combination with Prussian blue staining. Sections were scanned to confirm iron positive cells which were also positive for the MHC class II marker. Pictures were taken at 400 x magnification using a light microscope equipped with a digital camera.
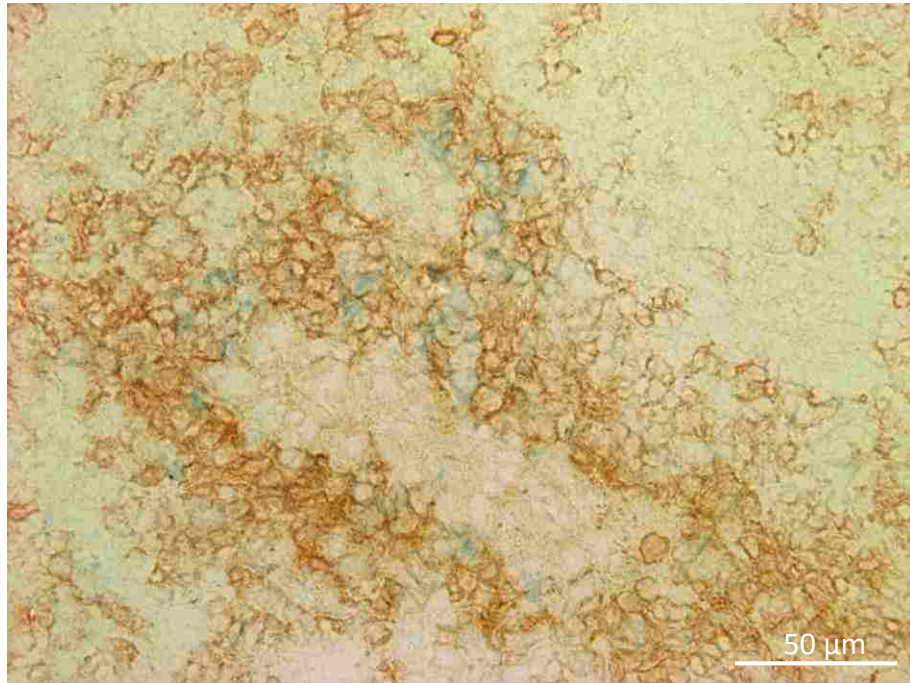
Figure 16. Iron oxide and Bu-1 (B cells) double staining in frozen spleen tissue sections from chickens injected intravenously with iron oxide nanoparticles. A 9-week-old Light-brown Leghorn female was intravenously injected with IO-COOH nanoparticles (dose of 3.3 mg/kg). Organs were collected 60 min post-intravenous injection. Frozen spleen sections (7 µm) were prepared and stained using indirect immunohistochemistry with chicken Bu-1 specific antibody in combination with Prussian blue staining. Pictures were taken at 400 x magnification using a light microscope equipped with a digital camera.
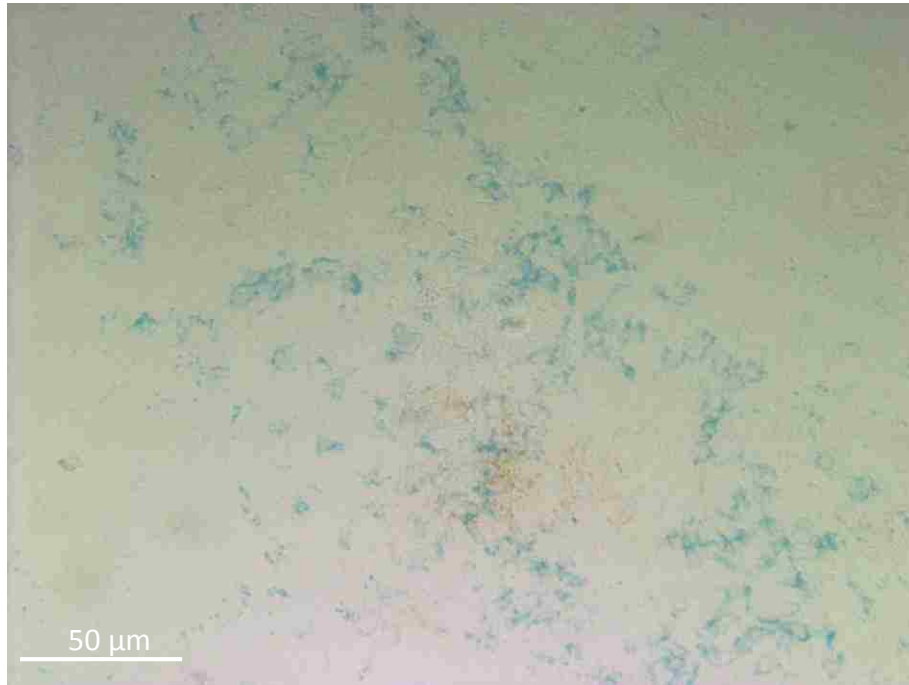
Figure 17. Iron oxide and isotype control double staining in frozen spleen tissue sections from chickens injected intravenously with iron oxide nanoparticles. A 9-week-old Light-brown Leghorn female was intravenously injected with IO-COOH nanoparticles (dose of 3.3 mg/kg). Organs were collected 60 min post-intravenous injection. Frozen spleen sections (7 μm) were prepared and stained using indirect immunohistochemistry with isotype control antibodies (mouse IgG1) in combination with Prussian blue staining. Sections were scanned to confirm iron positive cells and no non-specific binding of the cell-specific (mouse IgG1) antibodies used to identify macrophages, MHC-II+ cells, and B cells (no brown staining). Pictures were taken at 400 x magnification using a light microscope equipped with a digital camera.

DISCUSSION

Iron oxide (IO) nanoparticles are popular materials for use in the biomedical field. To be used in health care, the safety and effectiveness of nanoparticles needs to be tested in a living organism. For this project we used the chicken as the animal model to examine *in vivo* activities of nanoparticles, with focus on targeting/delivery of intravenously injected IO nanoparticles. The chicken model has advantages over other non-human animal models such as the mouse, including opportunity for easy blood sampling as well as the unique feature which is repeat, minimally invasive access to a complex dermal tissue in the form of growing feathers (Erf and Ramachandran, 2016). Before the targeting studies involving growing feathers as the target tissue could be carried out, a major part of this study was to examine the organ-distribution and circulatory half-life of intravenously injected iron oxide nanoparticles in the chicken. Determination of the presence of iron oxide nanoparticles in blood and organs at different time points post intravenous injection of nanoparticles provided the first insight into the *in vivo* behavior of the nanoparticles in the chicken system.

Iron concentration in plasma, serum, and homogenized tissues were first examined using two different commercial iron assay kits. Although the standard curves of both kits worked very well, iron concentration in plasma, serum, and homogenized tissue samples post IO injection were not different from pre-injection or PBS injected samples. Even when IO was added directly into plasma, serum, or whole blood, iron concentrations in plasma and serum samples collected were not detected or detected at much low levels than predicted. These results may be due to the test-kits not working with chicken serum and plasma samples, the iron oxide nanoparticles were removed from the blood within 5 minutes (the first time-point the blood was samples after i.v.

59

injection of IO nanoparticles), or the iron oxide nanoparticles were removed from the plasma/serum during the separation of the plasma/serum from the cell portion of the whole blood. The blood half-life of iron oxide nanoparticles depends on many factors including the type of animal injected, the type of iron oxide nanoparticles used, and doses of injected iron oxide nanoparticles (Arami et al., 2015). While there is no report about blood half-life of iron oxide nanoparticles in the avian system, many reports showed the blood half-life in rodents and humans. The blood half-life of different iron oxide nanoparticles ranges from several minutes to several days in rodents and from 1 hour to 24 hours in humans (Weissleder et al., 1990; Yang et al., 2011; Taupitz et al., 2004; McLachlan et al., 1994). Citric acid-coated super paramagnetic iron oxide nanoparticles were rapidly cleared from circulation in the rat model, with a half-life of about 14.06 min (Trincu et al., 2015). In our study it is also likely that we did not get the assay system to work properly, despite many attempts to optimize the assays. This conclusion is based on observations when liver homogenates known to have taken up IO nanoparticles (based on histology) were prepared and the iron was still not successfully detected using the assay kits. More research is needed to find a procedure and experimental approach that will better determine the circulatory half-life of IO nanoparticles injected i.v. in chickens.

The other approach used in this study was to examine the presence of iron oxide nanoparticles, specifically IO-COOH and IO-PEG, in organs (liver, spleen, kidney, and lung) before (0) and at 5, 15, 30, and 60 min post i.v. injection. At each time-point, formalin-fixed tissue samples were paraffin-embedded and sections were prepared and stained with Prussian blue iron stain. Sections were observed under a light microscope system, and pictures were taken at 100 x and 400 x magnification. While lung and kidney showed no iron-stained cells (blue cells) (Figure 3), liver and spleen showed many iron-stained cells in the sections (Figure 4).

Further examination of Prussian blue stained tissue sections showed iron staining (% Area) increased in spleen sections when the amount of intravenously injected IO increased (P < 0.05) (Figure 7). This is consistent with a demonstration that number of macrophages in mouse liver and spleen taking up IO nanoparticles linearly increased depending on the dose of IO nanoparticles injected (Rodrigues et al., 2017). However, in chickens, the correlation between dosage of IO nanoparticles injected intravenously and iron staining in the liver was not significant for the small range of doses tested. When compared to IO-COOH injection, IO-PEG injection using the same dosage of nanoparticles showed significantly lower % Area of iron staining and number of iron-positive cells at each time point post injection (Figure 7 and 8). By 60 min, % Area of iron staining in spleen sections from chickens injected with IO-PEG was approximately 8 times less than the % Area observed in spleen following intravenous IO-COOH injection (Figure 7). For the liver, however, iron staining (% Area and number of iron+ cells) in IO-PEG injected chickens was similar to that in IO-COOH injected chickens at the 60 min time point, although iron staining in IO-PEG injected chickens was much lower at earlier points than observed with IO-COOH injection (Figure 7 and 8). These results demonstrated that uptake of IO-PEG nanoparticles in chickens was slower in liver and spleen, and occurred at lower levels in the spleen, than uptake of IO-COOH nanoparticles. This observation is in line with the goals of PEG modification of iron oxide nanoparticles, specifically to reduce their capture by the body's immune system components and to extend their circulatory half-life (Yu et al., 2012; Chen et al, 2010).

For intravenously administered nanoparticles, the surface charge of nanoparticles is one of the factors affecting bio-distribution and clearance (Melancon et al., 2009). IO nanoparticles used in this study were IO-COOH nanoparticles which had reactive carboxylic groups on the

surface with negative charges; whereas, IO-PEG nanoparticles were iron oxide nanoparticles coated with poly-ethylene-glycol (PEG) with no linkable reactive group. Charged nanoparticles are easily cleared from the blood because they are quickly absorbed by serum proteins onto their surface, that tag them for removal by the mononuclear phagocytic system inside the liver and spleen (Lynch and Dawson, 2008). Deng and colleagues, in their article, declared that both negatively and positively charged gold nanoparticles had a wide range of proteins bound to their surface with high affinity, while the neutral nanoparticles had a very little bound proteins (Deng et al., 2013). On the other hand, some reports showed that the addition of PEG to the surface of nanoparticles increased the blood half-life of the nanoparticles regardless of surface charge (Gref et al., 2000; Owens and Peppas, 2006; Zhang et al., 2009). These above reports are in agreement with the results of IO-COOH and IO-PEG injection in the chicken system.

When the IO nanoparticle organ uptake data obtained by image analysis (% Area of iron staining) and by manual counting of iron positive cells were compared, highly significant correlations were found, revealing consistent results obtained by both methods (Figure 9). While counting of cells was more time consuming, it may be the more sensitive method in detecting IO nanoparticle uptake. For example, a significant increase in the number of iron-positive cells in livers from IO-PEG injected chickens was already observed at 30 minutes post i.v. injection, while image analysis did not find a significant increase in iron-staining until the 60 minute time point. On the other hand, if there are a lot of overlapping cells, as in the case for spleen from IO-COOH injected birds, the cell counting method was not possible, and the image analysis quantified the iron staining much more effectively (Figure 7 and 8).

In addition to the Prussian blue iron staining method, the peroxidase mimicking activity of iron oxide nanoparticles was also used to detect iron oxide nanoparticles in frozen tissue sections. This staining revealed elongated and spread-out cells that contained brown precipitant from DAB oxidation in livers from chickens injected with IO-COOH. There were many brown particles in the cytoplasm of the liver cells (Figure 10a) while there were no brown stained cells in liver sections of PBS injected chickens (Figure 10b). This result is consistent with the result of Prussian blue staining and previous report (Zhuang et al., 2012), confirming that this staining method can also identify cells that have taken up iron oxide nanoparticles and that iron oxide nanoparticles possess intrinsic peroxidase mimicking activity; i.e. iron oxide nanoparticles catalyze the oxidation of the peroxidase substrate DAB in the presence of H_2O_2 to produce a brown color. This poses a great potential for novel applications of iron oxide nanoparticles in different fields, especially biomedicine for construction of diagnostic kits and enzyme immunoassays (Wei and Wang, 2013; Hamid and Khalil, 2009). Moreover, the staining using peroxidase mimicking activity was suggested to be a better and more sensitive method than Prussian blue (Zhuang et al., 2012). The endogenous ferric iron in tissue usually affects Prussian blue results (Poss and Tonegawa, 1997) while this iron exhibits very little peroxidase activity (Gao et al., 2007). However, it should be noted that we were not able to identify iron-positive cells in spleen using this method. It appears that for this organ, where nanoparticles accumulate in cells within the marginal zone surrounding the white pulp lymphoid areas, this staining method may need to be further modified for the avian model.

In order to identify the cells in liver and spleen that have taken up the IO nanoparticles, we combined immunohistochemical staining with antibodies specific for chicken macrophages, MHC class II molecules and B cells, with Prussian blue staining of iron. The monoclonal

antibodies used to identify the leukocyte markers, do however not work with formalin fixed tissues. Therefore, we needed to work out Prussian blue staining on frozen tissue sections and design a staining procedure where the additional fixation step needed for Prussian blue staining would not interfere with the immunohistochemical staining. This was successfully achieved and revealed MHC class II+ macrophages (presumably Kupffer cells) in the liver as the cells that take up iron-oxide nanoparticles (Figure 11-13). This staining approach was again not as successful for spleen tissue sections, especially with the macrophage-specific antibody (Figure 14), although the iron staining in combination with the isotype control monoclonal antibodies clearly showed iron staining and the absence of non-specific binding of the monoclonal antibodies (Figure 17). In spleen, the dual staining with MHC class II specific monoclonal antibody and Prussian blue staining was more successful, revealing iron staining associated with MHC class II staining (Figure 15). Because B cells, which are located in follicles adjacent to the marginal zone are also MHC class II positive, double staining with antibody for B cells was also conducted. As seen in Figure 16, B cells do not appear to take up IO nanoparticles based on the presence of iron staining between, not in, B cells. Although for spleen, further modification of the staining procedures are needed to identify macrophages (e.g. immunofluorescent staining), based on Prussian blue staining, H/E staining, morphology and location of the iron positive cells within the spleen, the iron positive cells appear to be marginal zone macrophages. In fact, spleen and liver are two large units of the mononuclear phagocytic system (MPS) which include primarily monocytes and macrophages, both of which express MHC class-II molecules on their surface in addition to the KUL-01 macrophage marker. The observation that iron oxide nanoparticles were taken up rapidly by macrophages in the spleen and liver is in agreement with Zhuang et al. (2012) who reported that iron oxide nanoparticles were taken up mainly by liver

macrophages and macrophages in the perifollicular areas in spleen. Although this conclusion by Zhuang et al. was based on adjacent sections stained with different stains, i.e. one with iron stain the other with H/E stain, and not dual staining on the same sections. Chicken lung and kidney displayed no iron staining at all time points examined for both IO nanoparticle groups. This agrees with previous findings of minimal nanoparticle deposition in these organs (Tate et al., 2009).

Having the first insight into *in vivo* behavior of the IO nanoparticles in the chicken, set the stage for the targeting/delivery study using the growing feather as the target tissue for intravenously injected IO nanoparticles. In this model, the mouse IgG antigen was injected into the pulp of the chicken's growing feathers 6 hours before intravenous injection of antibody-conjugated IO nanoparticles. Specifically, the IO nanoparticles were conjugated with chicken-IgG antibody specific to the mouse-IgG-antigen injected into the dermis of growing feathers. The mouse-IgG injected growing feathers were then periodically sampled and examined for the presence of nanoparticles. Prussian blue stained tissue sections of mouse-IgG-antigen injected growing feathers showed no iron positive cells (blue cells) at any of the time-points examined. There are many reasons this first study was not successfully demonstrating the potential usefulness of the growing feather dermal tissue to study nanoparticle targeting delivery, including the choice of the antigen-antibody combination. Chicken-IgG-specific-to-mouse-IgG-antibody was chosen for intravenous injection in this study since the injection was in chicken and an immune response to the chicken antibody was therefore not expected. The chicken anti-mouse IgG antibody was commercially available. In addition, mouse IgG injected into the dermis of growing feathers was known to cause immune activities, including vascular changes favorable for nanoparticle entry from blood into injected growing feathers, by the 6 hour time-point.

Moreover, Prussian blue staining of IO nanoparticle injected growing feathers clearly showed uptake of the particles by macrophages (data not shown), supporting the concept that if i.v. injected IO nanoparticles leave the circulation to enter antigen-injected dermal tissue we would be able to detect them. However, arrival and retention of IO nanoparticles in the pulp of antigen-injected growing feathers could not successfully be demonstrated in this study.

Other possible reasons for this failure include the possibility that the mouse-IgG injected into growing feathers was already removed and taken up by inflammatory cells and hence not accessible to the antibody-conjugated iron oxide nanoparticles at the 6 hour time-point. Although as seen in H/E stained sections, the injection of mouse IgG into the dermis of the growing feathers did induce an inflammatory response including vascular changes that enabled extravasation of inflammatory leukocytes from the blood that also would have allowed nanoparticles to leave the circulation at this location. It is possible that the inflammatory response and associated vascular changes were not strong enough to have antibody-conjugated IO nanoparticles or unconjugated IO-PEG, or IO-COOH come into the tissue in large amounts. Perhaps, dual administration of specific antigen with low levels of lipopolysaccharide may have been a more favorable inflammatory stimulus for IO nanoparticle entry into the tissue. Lastly, the dosage of IO nanoparticles injected was lower than that used for targeting in other animal models (Chertok et al., 2008; NDong et al., 2015).

Conclusion

This is the first report describing organ-distribution of iron oxide nanoparticles in the chicken system, demonstrating accumulation of iron oxide nanoparticles in macrophages in liver and spleen, as well as differences in the time-course and uptake level of 10 nm IO-COOH

compared to 10 nm IO-PEG nanoparticles. Several protocols were successfully developed for the chicken model, including image analysis of tissue sections to quantify iron staining and manual counting of iron stained cells. Furthermore, protocols for staining frozen tissue sections using the peroxidase mimicking activity of IO nanoparticles, the Prussian blue HT20 staining kit, as well as a dual immunohistochemical and iron staining procedure were developed. Lastly while not successful, the targeting experiment conducted in this study is a very good starting point for experimental modifications to optimize this approach to monitor targeting/delivery success of nanoparticles.

REFERENCES

Abdul-Careem, M. F., Hunter, B. D., Sarson, A. J., Parvizi, P., Haghighi, H. R., Read, L., Heidari, M., and S. Sharif. 2008. Host responses are induced in feathers of chickens infected with Marek's disease virus. Virology. 370:323-332. doi:10.1016/j.virol.2007.09.013.

Abraham, S. A., Waterhouse, D. N., Mayer, L. D., Cullis, P. R., Madden, T. D., and M. B. Bally. 2005. The liposomal formulation of doxorubicin. Methods in Enzymology. 391:71-97. doi:10.1016/S0076-6879(05)91004-5.

Alexiou, C., Arnold, W., Klein, R. J., Parak, F. G., Hulin, P., Bergemann, C., Erhardt, W., Wagenpfeil, S., and A. S. Lubbe. 2000. Locoregional cancer treatment with magnetic drug targeting. Cancer Research. 60:6641-6648.

Arami, H., Khandhar, A., Liggitt, D., and K. M. Krishnan. 2015. In vivo delivery, pharmacokinetics, biodistribution and toxicity of iron oxide nanoparticles. Chemical Sociaty Review. 44:8576-8686. doi:10.1039/c5cs00541h.

Attaluri, A., Kandala, S. K., Wabler, M., Zhou, H., Cornejo, C., Armour, M., Heydayati, M., Zhang, Y., Deweese, T. L., Herman, C., and R. Ivkov. 2015. Magnetic nanoparticle hyperthermia enhances radiation therapy: A study in mouse models of human prostate cancer. International Journal of Hyperthermia. 31:359-374. doi:10.3109/02656736.2015.1005178.

Bai, F., Wang, C., Lu, Q., Zhao, M., Ban, F., Yu, D., Guan, Y., Luan, X., Liu, Y., Chen, H., and C. Fang. 2013. Nanoparticle-mediated drug delivery to tumor neovasculature to combat P-gp expressing multidrug resistant cancer. Biomaterials. 34:6163-6174. doi:10.1016/j.biomaterials.2013.04.062.

Barenholz, Y. 2012. Doxil(R)-the first FDA-approved nano-drug: lessons learned. Journal of Control Release. 160:117-134. doi:10.1016/j.jconrel.2012.03.020.

Bhuyan, D., Arbuj, S. S., and L. Saikia. 2015. Template-free synthesis of Fe3O4 nanorod bundles and their highly efficient peroxidase mimetic activity for the degradation of organic dye pollutants with H2O2. New Journal of Chemistry. 39:7759-7762. doi:10.1039/c5nj01918d.

Chaudhari, K. N., Chaudhari, N. K., and J. Yu. 2012. Peroxidase mimic activity of hematite iron oxides (α-Fe2O3) with different nanostructures. Catalysis Science and Technology. 2:119-124. doi:10.1039/c1cy00124h.

Chen, Y., Tao, J., Xiong, F., Zhu, J., Gu, N., and K. Geng. 2010. Characterization and in vitro cellular uptake of PEG coated iron oxide nanoparticles as MRI contrast agent. Pharmazie. 65:481-486. doi:10.16 91/ph.2010.9372.

Chertok, B., Moffat, B. A., David, A. E., Yu, F., Bergemann, C., Ross, B. D., and V. C. Yang. 2008. Iron oxide nanoparticles as a drug delivery vehicle for MRI monitored magnetic targeting of brain tumors. Biomaterials. 29:487-496. doi: 10.1016/j.biomaterials.2007.08.050.

Chin, S. H., Bum, J. S., and Y. W. Kim. 2013. Selective dermal rejuvenation using intradermal injection of carbon dioxide and hyaluronic acid for facial wrinkles. Annals of Plastic Surgery. 70:628-631. doi: 10.1097/SAP.0b013e31823fa958.

Clemente-Casares, X., and P. Santamaria. 2014. Nanomedicine in autoimmunity. Immunol Letters. 158:167-174. doi:10.1016/j.imlet.2013.12.018.

Crawford, C. L. 2017. A skin test for latent tuberculosis. South African Medical Journal. 107:362-362. doi: 0.7196/SAMJ.2017.v107i5.12380.

Davison, T. F., Kaspers, B., and K. A. Schat. 2008. Avian immunology. 496. Amsterdam, Boston: Academic Press.

Deng, Z. J., Liang, M., Toth, I., Monteiro, M., and R. F. Minchin. 2013. Plasma protein binding of positively and negatively charged polymer-coated gold nanoparticles elicits different biological responses. Nanotoxicology. 7:314–322. doi:10.3109/17435390.2012.655342.

Erf, G. F., Falcon, D. M., Sullivan K. S., and S. E. Bourdo. 2017. T lymphocytes dominate local leukocyte infiltration in response to intradermal injection of functionalized graphene-based nanomaterial. Journal of Applied Toxicology. doi:10.1002/jat.3492. (in press).

Erf, G. F., and I. R. Ramachandran. 2016. The growing feather as a dermal test site: Comparison of leukocyte profiles during the response to Mycobacterium butyricum in growing feathers, wattles, and wing webs. Poultry Science. 95:2011-2022. doi:10.3382/ps/pew122.

Erf, G. F., Trejoskalli, A., and J. Smyth. 1995. T-cells in regenerating feathers of Smyth line chickens with vitiligo. Clinical Immunology and Immunopathology. 76:120-126. doi:10.1006/clin.1995.1105.

Falzarano, M. S., Bassi, E., Ferlini, A., Passarelli, C., and P. Braghetta. 2014. Biodistribution studies of polymeric nanoparticles for drug delivery in mice. Human Gene Therapy. 25:927-928. doi:10.1089/hum.2014.073.

Fu, G., Sanjay, S. T., and X. Li. 2016. Cost-effective and sensitive colorimetric immunosensing using an iron oxide to prussian blue nanoparticle conversion strategy. Analyst. 141: 3883-3889. doi:10.1039/c6an00254d.

Gao, L., Zhuang, J., Nie, L., Zhang, J., Zhang, Y., Gu, N., Wang, T., Feng, J., Yang, D., Perrett, S., and X. Yan. 2007. Intrinsic peroxidase-like activity of ferromagnetic nanoparticles. Nature Nanotechnology. 2:577 − 583. doi:10.1038/nnano.2007.260.

Gref, R., Luck, M., Quellec, P., Marchand, M., Dellacherie, E., Harnisch, S., Blunk, T., and R. H. Muller. 2000. 'Stealth' corona-core nanoparticles surface modified by polyethylene glycol (PEG): influences of the corona (PEG chain length and surface density) and of the core composition on phagocytic uptake and plasma protein adsorption. Colloids and Surfaces B: Biointerfaces.18:301-313. doi:org/10.1016/S0927-7765(99)00156-3.

Hamid, M., and Khalil-ur-Rehman. 2009. Potential applications of peroxidases. Food Chemistry. 115:1177–1186. doi:10.1016/j.foodchem.2009.02.035.

Hawkins, M. J., Soon-Shiong, P., and N. Desai. 2008. Protein nanoparticles as drug carriers in clinical medicine. Advanced Drug Delivery Reviews. 60:876-885. doi:10.1016/j.addr.2007.08.044.

Jarockyte, G., Daugelaite, E., Stasys, M., Statkute, U., Poderys, V., Ting-Chen T., Shan-Hui H., Karabanovas, V., and R. Rotomskis. 2016. Accumulation and toxicity of superparamagnetic iron oxide nanoparticles in cells and experimental animals. International Journal of Molecular Sciences. 17:1-13. doi:10.3390/ijms17081193.

Koo, H., Huh, M., Sun, I., Yuk, S., Choi, K., Kim, K., and I. Kwon. 2011. In vivo targeted delivery of nanoparticles for theranosis. Accounts of Chemical Research. 44:1018-1028. doi:10.1021/ar2000138.

Lartigue, L., Wilhelm, C., Servais, J., Factor, C., Dencausse, A., Bacri, J., Luciani, N., and F. Gazeau. 2012. Nanomagnetic sensing of blood plasma protein interactions with iron oxide nanoparticles: Impact on macrophage uptake. ACS Nano. 6:2665-2678. doi:10.1021/nn300060u.

Lu, M., Cohen, M. H., Rieves, D., and R. Pazdur. 2010. FDA report: Ferumoxytol for intravenous iron therapy in adult patients with chronic kidney disease. American Journal of Hematology. 85:315-319. doi: 10.1002/ajh.21656.

Lucas, M. A., and P. R. Stettenheim. 1972. Avian Anatomy: Integument. Agriculture Handbook 362. United States Department of Agriculture, U. S. Government Printing Office, Washington, DC.

Lynch, I., and K. A. Dawson. 2008. Protein-nanoparticle interactions. Nano Today. 104:2050-2055. doi:org/10.1016/S1748-0132(08)70014-8Get rights and content.

Mahdavi, M., Bin Ahmad, M., Haron, M., Namvar, F., Nadi, B., Ab Rahman, M., and J. Amin. 2013. Synthesis, surface modification and characterization of biocompatible magnetic iron oxide nanoparticles for biomedical applications. Molecules. 18:7533-7548. doi:10.3390/molecules18077533.

McLachlan, S. J., Morris, M. R., Lucas, M. A., Fisco, R. A., Eakins, M. N., Fowler, D. R., Scheetz, R. B., and A. Y. Olukotun. 1994. Phase I clinical evaluation of a new iron oxide MR contrast agent. Journal of Magnetic Resonance. 4:301–307. doi:10.1002/jmri.1880040313.

Mahmoudi, M., Sant, S., Wang, B., Laurent, S., and T. Sen. 2011. Superparamagnetic iron oxide nanoparticles (SPIONs): Development, surface modification and applications in chemotherapy. Advanced Drug Delivery Reviews. 63:24-46. doi:10.1016/j.addr.2010.05.006.

Melancon, M. P., Lu, W., and C. Li. 2009. Gold-Based Magneto/Optical Nanostructures: Challenges for In Vivo Applications in Cancer Diagnostics and Therapy. Materials Research Bulletin. 34:415–421. doi:https://doi.org/10.1557/mrs2009.117.

Miele, E., Spinelli, G. P., Miele, E., Tomao, F., and S. Tomao. 2009. Albumin-bound formulation of paclitaxel (Abraxane ABI-007) in the treatment of breast cancer. Internatinal Journal of Nanomedicine. 4:99-105. doi: 10.2147/IJN.S3061.

Mitragotri, S., Burke, P. A., and R. Langer. 2014. Overcoming the challenges in administering biopharmaceuticals: formulation and delivery strategies. Nature Reviews Drug Discovery. 13:655-672. doi:10.1038/nrd4363.

Muthiah, M., Park, I., and C. Cho. 2013. Surface modification of iron oxide nanoparticles by biocompatible polymers for tissue imaging and targeting. Biotechnology Advances. 31:1224-1236. doi:10.1016/j.biotechadv.2013.03.005.

NDong, C., Tate, J. A., Kett, W. C., Batra, J., Demidenko, E., Lewis, L. D., Hoopes, P. J., Gerngross, T. U., and K. E. Griswold. 2015. Tumor cell targeting by iron oxide nanoparticles is dominated by different factors *in vitro* versus *in vivo*. *PLoS ONE*, *10*(2). doi:10.1371/journal.pone.0115636.

Nickels, A. S., Li, J. T., and G. Volcheck. 2014. Percutaneous and intradermal allergy skin test utilization in the United States 2012 Medicare population. Journal of Allergy and Clinical Immunology in Practice. 2:807-809. doi:10.1016/j.jaip.2014.07.010.

Owens, D. E., and N. A. Peppas. 2006. Opsonization, biodistribution, and pharmacokinetics of polymeric nanoparticles. International Journal of Pharmaceutics. 307:93-102. doi:10.1016/j.ijpharm.2005.10.010.

Pedro, T., María del Puerto, M., Sabino, V.-V., Teresita, G.-C., and J. S. Carlos. 2003. The preparation of magnetic nanoparticles for applications in biomedicine. Journal of Physics D: Applied Physics. 36:182-197. doi:10.1088/0022-3727/36/13/202.

Poss, K. D., and S. Tonegawa. 1997. Reduced stress defense in heme oxygenase 1-deficient cells. Proceedings of the National Academy of Sciences of the United States of America. 94:10925-10930.

Pusic, K., Z. Aguilar, J. McLoughlin, S. Kobuch, H. Xu, M. Tsang, A. Wang, and G. Hui. 2013. Iron oxide nanoparticles as a clinically acceptable delivery platform for a recombinant blood-stage human malaria vaccine. The FASEB Journal. 27:1153-1166. doi: 10.1096/fj.12-218362.

Rodrigues, D., Freitas, M., Marisa Costa, V., Arturo Lopez-Quintela, M., Rivas, J., Freitas, P., Carvalho, F., Femandes, E., and P. Silva. 2017. Quantitative histochemistry for macrophage biodistribution on mice liver and spleen after the administration of a pharmacological-relevant dose of polyacrylic acid-coated iron oxide nanoparticles. Nanotoxicology. 11:256-266. doi:10.1080/17435390.2017.1291865.

Rodzinski, A., Guduru, R., Liang, P., Hadjikhani, A., Stewart, T., Stimphil, E., Runowicz, C., Cote, R., Altman, N., Datar, R., and S. Khizroev. 2016. Targeted and controlled anticancer drug delivery and release with magnetoelectric nanoparticles. 6:20867-20880. doi:10.1038/srep20867.

Rowinsky, E. K., and R. C. Donehower. 1995. Paclitaxel (taxol). The New England Journal of Medicine, 332:1004-1014. doi:10.1056/NEJM199504133321507.

Sajja, H. K., East, M. P., Mao, H., Wang, Y. A., Nie, S., and L. Yang. 2009. Development of multifunctional nanoparticles for targeted drug delivery and noninvasive imaging of therapeutic effect. Current Drug Discovery Technologies. 6:43-51. doi:10.2174/157016309787581066.

Salata, O. 2004. Applications of nanoparticles in biology and medicine. Journal of Nanobiotechnology, 2:3-8. doi:10.1186/1477-3155-2-3.

Shen, C., Liang, H., Wang, C., Liao, M., and T. Jan. 2011. A role of cellular glutathione in the differential effects of iron oxide nanoparticles on antigen-specific T cell cytokine expression. International Journal of Nanomedicine. 6:2791-2798. doi:10.2147/IJN.S25588.

Shi, F., B.-W. Kong, J. J. Song, J. Y. Lee, R. L. Dienglewicz, and G. F. Erf. 2012. Understanding mechanisms of spontaneous autoimmune vitiligo development in the Smyth line chicken model by transcriptomic microarray analysis of evolving lesions. BioMed Central Immunology 13:18; 1-15. doi:10.1186/1471-2172-13-18.

Sinani, V. A., Koktysh, D. S., Yun, B. G., Matts, R. L., Pappas, T. C., Motamedi, M., Thomas, S. N., and N. A. Kotov. 2003. Collagen coating promotes biocompatibility of semiconductor nanoparticles in stratified LBL films. Nano Letters. 3:1177-1182. doi:10.1021/nl0255045.

Strehl, C., Maurizi, L., Gaber, T., Hoff, P., Broschard, T., Poole, A., Hofmann, H., and F. Buttgereit. 2016. Modification of the surface of superparamagnetic iron oxide nanoparticles to enable their safe application in humans. International Journal of Nanomedicine. 11:5883-5896. doi:10.2147/IJN.S110579.

Sullivan, K. S., and G. F. Erf. 2017. CD4+ T cell dominate the leukocyte infiltration response initiated by intra-dermal injection of phytohemagglutinin into growing feather in chickens. Poultry Science. doi:10.3382/ps/pex135. (in press).

Sun, L., Huang, C., Gong, T., and S. Zhou. 2010. A biocompatible approach to surface modification: Biodegradable polymer functionalized super-paramagnetic iron oxide nanoparticles. Materials Science & Engineering c-Materials for Biological Applications. 30:583-589. doi:10.1016/j.msec.2010.02.009.

Tate, J. A., Ogden, J. A., Strawbridge, R. R., Pierce, Z. E., and P. J. Hoopes. 2009. Toxicity and biodistribution of activated and non-activated intravenous iron oxide nanoparticles. Proceedings of SPIE. 12:7181-71810L. doi: 10.1117/12.809830.

Taton, T. A. 2002. Nanostructures as tailored biological probes. Trends in Biotechnology. 20:277-279. doi: 10.1016/S0167-7799(02)01973-X.

Taupitz, M., Wagner, S., Schnorr, J., Kravec, I., Pilgrimm, H., Bergmann-Fritsch, H., and B. Hamm. 2004. Phase I clinical evaluation of citrate-coated monocrystalline very small superparamagnetic iron oxide particles as a new contrast medium for magnetic resonance imaging Investigative Radiology. 39:394–405. doi:10.1097/01.rli.0000129472.45832.b0.

Tavaré, R., Sagoo, P., Varama, G., Tanriver, Y., Warely, A., Diebold, S. S., Southworth, R., Schaeffter, T., Lechler, R. I., Razavi, R., Lombardi, G., and G. E. D. Mullen. 2011. Monitoring of in vivo function of superparamagnetic iron oxide labelled murine dendritic cells during anti- tumour vaccination. Plos One. 6:1-11. doi:10.1371/journal.pone.0019662.

Tiruppathi, C., Song, W., Bergenfeldt, M., Sass, P., and A. B. Malik. 1997. Gp60 activation mediates albumin transcytosis in endothelial cells by tyrosine kinase-dependent pathway. Journal of Biological Chemistry, 272:25968-25975. doi: 10.1074/jbc.272.41.25968.

Trincu, N. F., Balseanu, T. A., Ungureanu, B. S., Fifere, A., Pirici, I., Saftoiu, A., and J. Neamu. 2015. Blood Clearance of Citric Acid-Coated Superparamagnetic Iron Oxide Nanoparticles in Rats - a Pilot Study. Current Health Sciences Journal. 41:302-306. doi:10.12865/CHSJ.41.04.02.

Ulbrich, K., Knobloch, T., and J. ö. Kreuter. 2011. Targeting the insulin receptor: Nanoparticles for drug delivery across the blood-brain barrier (BBB). Journal of Drug Targeting. 19:125-132. doi:10.3109/10611861003734001.

Ungureanu, B. S., Margaritescu, C., Pirici, D., Gheonea, I. A., Trincu, N. F., Fifere, A., Tudorascu, D., and A. Saftoiu. 2015. Iron oxide nanoparticles biodistribution in an experimental pig model - A new approach for delivery and imaging. Current Health Sciences Journal. 41:333-338. doi:10.12865/CHSJ.41.04.07.

US patent 8,216,551. 2012. In vivo system to monitor tissue responses in birds. http://patft.uspto.gov/

Von Hoff, D. D., Ervin, T, Arena, F. P., Chiorean, E. G., Infante, J., Moore, M., Seay, T., Tjulandin, S. A., Ma, W. W., Saleh, M. N., Harris, M., Reni, M., Dowden, S., Laheru, D., Bahary, N., Ramanathan, R. K., Tabemero, J., Hidalgo, M., Goldstein, D., Cutsem, E. V., Wei,

X., Iglesias, J., and M. F. Renschler. 2013. Increased survival in pancreatic cancer with nab-paclitaxel plus gemcitabine. The New England Journal of Medicine. 369:1691-1703. doi:10.1056/NEJMoa1304369.

Wei, H., and E. Wang. 2013. Nanomaterials with enzyme-like characteristics (nanozymes): next-generation artificial enzymes. Chemical Society Reviews. 42:6060–6093. doi: 10.1039/C3CS35486E.

Weissleder, R., Elizondo, G., Wittenberg, J., Rabito, C. A., Bengele, H. H., and L. Josephson. 1990. Radiology. Ultrasmall superparamagnetic iron oxide: characterization of a new class of contrast agents for MR imaging. Radiology. 175:489–493. doi: 10.1148/radiology.175.2.2326474.

Wick, G., Andersson, L., Hala, K., Gershwin, M. E., Selmi, C., Erf, G. F., Lamont, S. J., and R. Sgonc. 2006. Avian models with spontaneous autoimmune diseases. Advances in Immunology. 92:71-117. doi:10.1016/S0065-2776(06)92002-1.

Wick, G., Backovic, A., Rabensteiner, E., Plank, N., Schwentner, C., and R. Sgonc. 2010. The immunology of fibrosis: Innate and adaptive responses. Trends in Immunology, 31:110-119. doi:10.1016/j.it.2009.12.001.

Woo, M., Kim, M., Jung, J., Park, K., Seo, T., and H. Park. 2013. A novel colorimetric immunoassay utilizing the peroxidase mimicking activity of magnetic nanoparticles. International Journal of Molecular Sciences. 14:9999-10014. doi:10.3390/ijms14059999.

Yang, H. W., Hua, M. Y., Liu, H. L., Huang, C. Y., Tsai, R. Y., Lu, Y. J., Chen, J. Y., Tang, H. J., Hsien, H. Y., Chang, Y. S., Yen, T. C., Chen, P. Y., and K. C. Wei. 2011. Self-protecting core-shell magnetic nanoparticles for targeted, traceable, long half-life delivery of BCNU to gliomas. Biomaterials. 32, 6523–6532. doi:10.1016/j.biomaterials.2011.05.047.

Yang, L., Cao, Z., Sajja, H., Mao, H., Wang, L., Geng, H., Xu, H., Jiang,T., Wood, W., Nie, S., and Y. Wang. 2008. Development of receptor targeted magnetic iron oxide nanoparticles for efficient drug delivery and tumor imaging. Journal of Biomedical Nanotechnology. 4:439-449. doi:10.1166/jbn.2008.007.

Yu, M., Huang, S., Yu, K., and A. Clyne. 2012. Dextran and polymer polyethylene glycol (PEG) coating reduce both 5 and 30 nm iron oxide nanoparticle cytotoxicity in 2D and 3D cell culture. International Journal of Molecular Sciences. 13:5554-5570. doi:10.3390/ijms13055554.

Yuan, Y., Rende, D., Altan, C. C., Bucak, S., Ozisik, R., and D. Borca-Tasciuc. 2012. Effect of surface modification on magnetization of iron oxide nanoparticle colloids. Langmuir. 28:13051-13059. doi:10.1021/la3022479.

Zhang, G., Yang, Z., Lu, W., Zhang, R., Huang, Q., Tian, M., Li, L., Liang, D., and C. Li. 2009. Influence of anchoring ligands and particle size on the colloidal stability and in vivo

biodistribution of polyethylene glycol-coated gold nanoparticles in tumor-xenografted mice. Biomaterials. 30:1928-1936. doi:10.1016/j.biomaterials.2008.12.038.

Zhuang, J., Fan, K., Gao, L., Lu, D., Feng, J., Yang, D., Gu, N., Zhang, Y. Liang, M., and X. Yan. 2012. Ex vivo detection of iron oxide magnetic nanoparticles in mice using their intrinsic peroxidase-mimicking activity. Molecular Pharmaceutics. 9:1983-1989. doi:10.1021/mp300033a.

APPENDICES